Computers and Mathematics with Applications 70 (2015) 1852–1877

Contents lists available at ScienceDirect

Computers and Mathematics with Applications

journal homepage: www.elsevier.com/locate/camwa

Topology optimization considering fatigue life in the frequency domain

Jong Wook Lee [a], Gil Ho Yoon [b,*], Seung Hyun Jeong [a]

[a] Graduate School of Mechanical Engineering, Hanyang University, Republic of Korea
[b] School of Mechanical Engineering, Hanyang University, Seoul, Republic of Korea

ARTICLE INFO

Article history:
Received 3 March 2015
Received in revised form 9 July 2015
Accepted 1 August 2015
Available online 24 August 2015

Keywords:
Topology optimization
Fatigue life
Narrow band solution
Wirsching and Light method
Ortiz and Chen method
Dirlik method

ABSTRACT

This research develops a new topological optimization (TO) method to assess dynamic fatigue failure in the frequency domain for random excitation forces. Besides static failure, fatigue life (or fatigue failure) is an important design criterion for the safety of mechanical and building structures. Therefore, many assessment theories and computational approaches have been proposed, and they can be divided into two categories: time domain and frequency domain. Although both approaches have been successfully applied for engineering purposes, they are rarely considered in structural TO. To consider fatigue failure caused by stochastic mechanical loads in structural TO, this research adopts fatigue assessment approaches in the frequency domain, such as narrow band solution, the Wirsching and Light method, the Ortiz and Chen method, and Dirlik method. For TO, we perform an adjoint sensitivity analysis with those fatigue assessment methods. We consider some two-dimensional benchmark problems and show that the present design method successfully constrains fatigue.

1. Introduction

This research presents a new topology optimization (TO) method that can consider fatigue life in the frequency domain. In addition to static failure, fatigue life or fatigue failure is an important design criterion for the safety of mechanical and building structures, as shown in Fig. 1. When a mechanical structure is excited by an arbitrary dynamic load, some cracks arise inside the structure, and those cracks can eventually cause the fracture of the structure. Thus many assessment theories and computational approaches have been proposed, and they can be divided into two categories: time domain and frequency domain. Although they have been successfully applied for engineering purposes, they are rarely considered in structural TO. Thus, this study contributes to this research area by developing an optimization formulation and modifying these theories and approaches to make them suitable for structural optimization.

Fatigue life, which is the time before a sudden fracture, can be assessed in the time or frequency domain [1–9]. The rain flow counting method is generally accepted as the standard approach in the time domain. However, its application is limited to a relatively simple load profile and a short time period. To consider complex load profiles for a long time span, applied loads should be analyzed in the frequency domain with the S–N curve. Some assessment methods have already been developed [3–9]. These methods calculate the PSD (power spectrum density) function and PDF (probability density function) of applied loads; their features are briefly explained in the subsequent sections, or see [3,4,8,9] for more details. Using PSD and PDF, the

* Corresponding author.
E-mail addresses: ghy@hanyang.ac.kr, gilho.yoon@gmail.com (G.H. Yoon).

http://dx.doi.org/10.1016/j.camwa.2015.08.006
0898-1221/

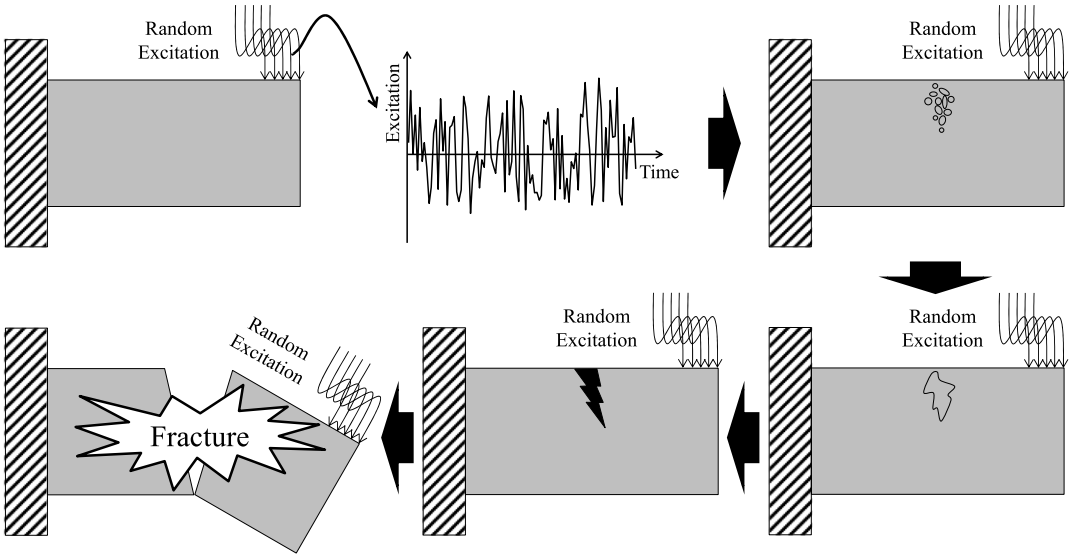

Fig. 1. General fatigue progress process.

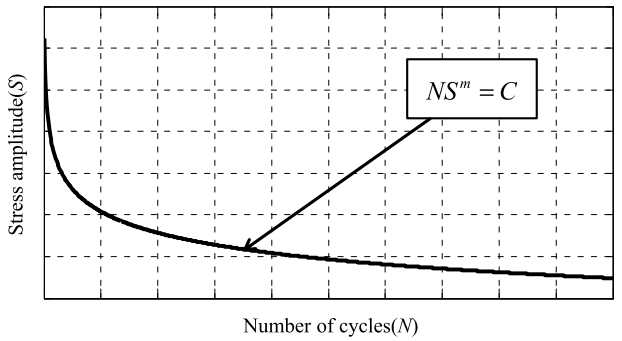

Fig. 2. S–N curve for fatigue analysis.

time history information of applied loads can be analyzed in the frequency domain, making it easy to analyze a complex load over a long time. The load profiles in the frequency domain are further divided into the narrow band frequency region and the wide band frequency region, depending on the frequencies of the focused applied load. The assessment in the narrow band frequency region was first proposed in [3,4,8,9], and it is called the *narrow band solution* [3,4,8,9]. Although this narrow band solution is efficient and conceptually easy to understand, it neglects information from the wide band frequency region, and its assessment is conservative. To overcome those limitations, many new approaches, such as the Wirsching and Light method, the Ortiz and Chen method, and Dirlik method, have been proposed [5–7].

From a structural optimization point of view, it is important to consider both fatigue failure and static failure. Much research has already been done to address structural failures [10–28]. The consideration of local failures in TO is especially difficult, and much research has been conducted. However, researchers rarely consider the fatigue constraint in structural TO, which allows free-material distribution [27,29–31].

TO was proposed in [32,33], and it has been applied to various application areas [34–38]. Because it allows free-material distribution, it can provide much better initial designs than the size or shape optimization methods. Despite its dissemination in various multiphysics systems, its application to the failure constraint is still a difficult problem because of stress singularity, the local constraint issue, and nonlinear behavior. Thus, many innovative ideas such as *qp*-relaxation, the *p*-norm approach, and regional constraints have been proposed to resolve these issues [10–12,14–18,21,22,26,39]. Recently, static failure for ductile and brittle materials and the dynamic fatigue constraint for harmonic load (one-frequency load) have been considered in TO [26,27]. But it remains difficult to consider complicated dynamic loads. To contribute to these research fields and consider complex load profiles over a long time period, this research applies fatigue life assessments in the frequency domain to TO. Similar to structural TO for static failure, many theoretical difficulties, such as the local constraint, stress singularity, and nonlinear constraint issues, occur in the fatigue constraint in the frequency domain of interest. To resolve them, the *qp*-relaxation approach and the *p*-norm approach have been applied, which permits the structural TO problem to be solved with consideration of fatigue failure in the frequency domain.

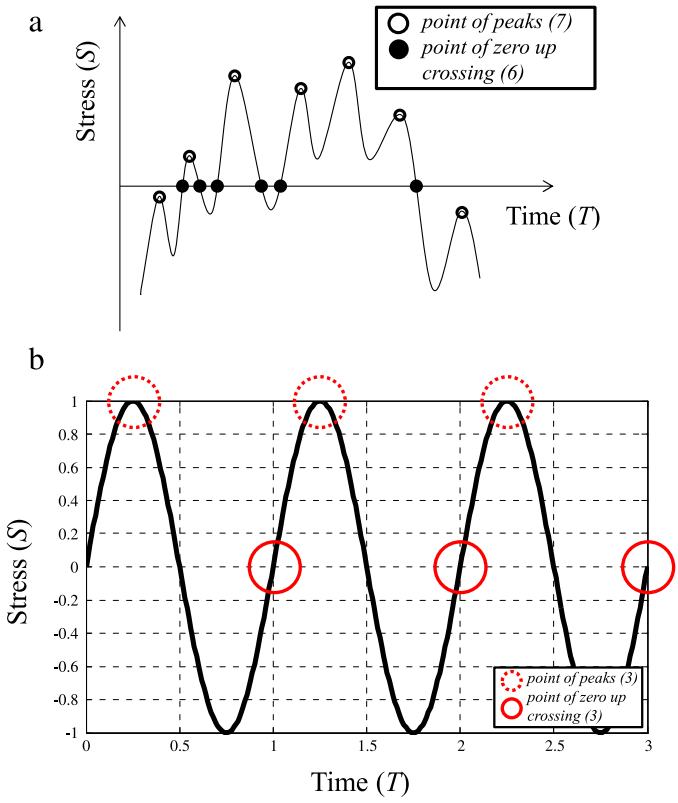

Fig. 3. An illustrative example of peaks and upward zero crossing for a random excitation. (a) The concepts of E_p and E_{0^+} ($E_p \cong 7,\ E_{0^+} \cong 3$) and (b) the case of a harmonic load ($E_p = 3,\ E_{0^+} = 3$).

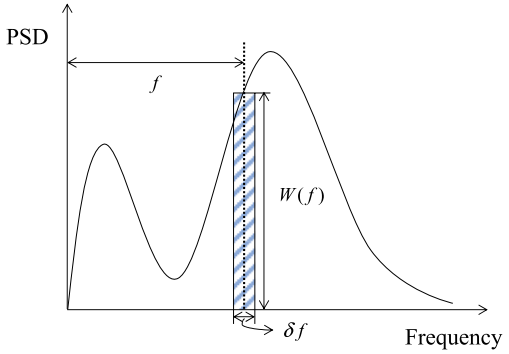

Fig. 4. Power spectrum density function.

This paper is organized as follows: in Section 2, we explain fatigue life estimation approaches in the frequency domain and modify those approaches for TO. We present and derive a new TO formulation and sensitivity analysis for the fatigue constraint with respect to the design variables in Section 3. In Section 4, we solve several numerical examples to show the effectiveness of our formulation. In Section 5, we provide our conclusions and findings.

2. Fatigue life estimation

In this section, we explain the estimation approaches for fatigue life in the frequency domain before we develop a new TO formulation constraining fatigue life. One of the distinct advantages of the estimations of fatigue life in the frequency domain is that they can consider fatigue life caused by non-proportional loads that change their principal axes, whereas the fatigue life methods in the time domain cannot consider the effect of non-proportional loads. It is important to use some special estimation approaches for the calculations of the equivalent stress such as Langer criterion, modified Langer criterion, and Lee criterion [40]. However in the present research, as we adopt the von-Mises stress for the calculations

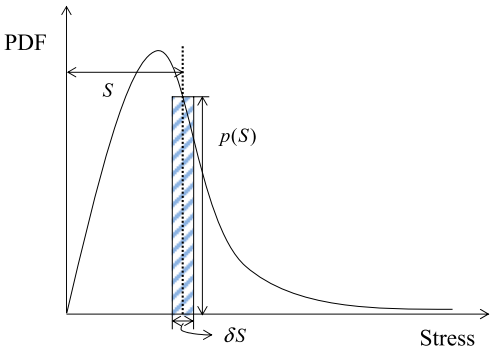

Fig. 5. Probability density function.

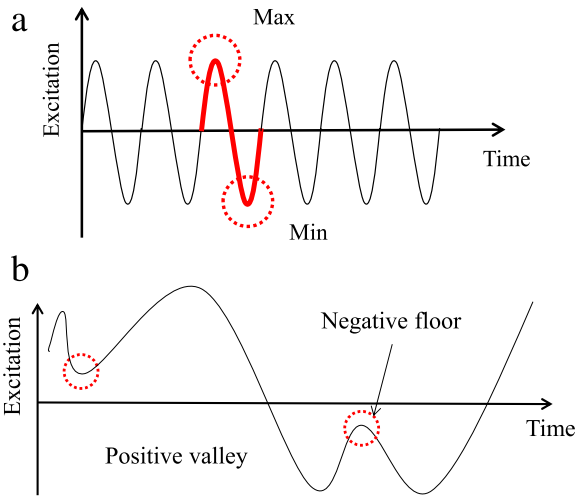

Fig. 6. Peak count by the narrow band solution.

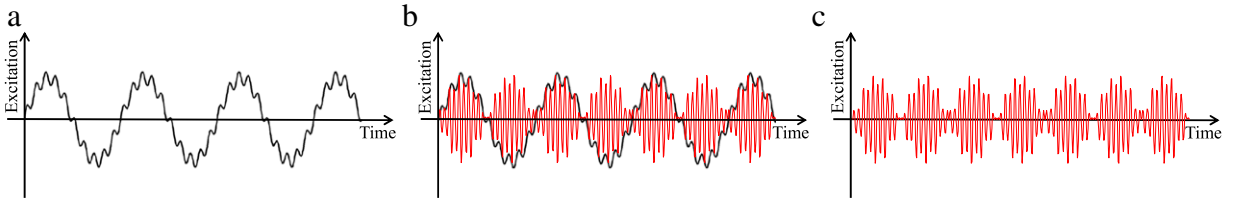

Fig. 7. A limitation of the narrow band solution [4,8]. (a) An original load history, (b) a load profile by the narrow band solution, and (c) a load history by the narrow band solution. (See [4,8] for more details.)

of the equivalent stress, the non-proportional loads are not considered. Furthermore, as they are based on the frequency domain, it is relatively easy to consider random vibration or random excitation. Here, however, we consider a relatively simple excitation as an illustration.

2.1. Fatigue life estimation in the frequency domain

When an isotropic structure is subjected to repetitive mechanical loads less than its ultimate stress, micro and macro cracks develop, accumulate, and progress inside the structure. If the number of repeated loads exceeds certain limitations, the structure will fracture. Therefore, in an engineering design process, it is important to know or predict the cycle numbers of repeated mechanical loads as well as their magnitude. To address the accumulated damage, the standard approach is to apply following Miner's rule.

$$D = \sum_{i=1}^{kn} \frac{n_i}{N_i} \tag{1}$$

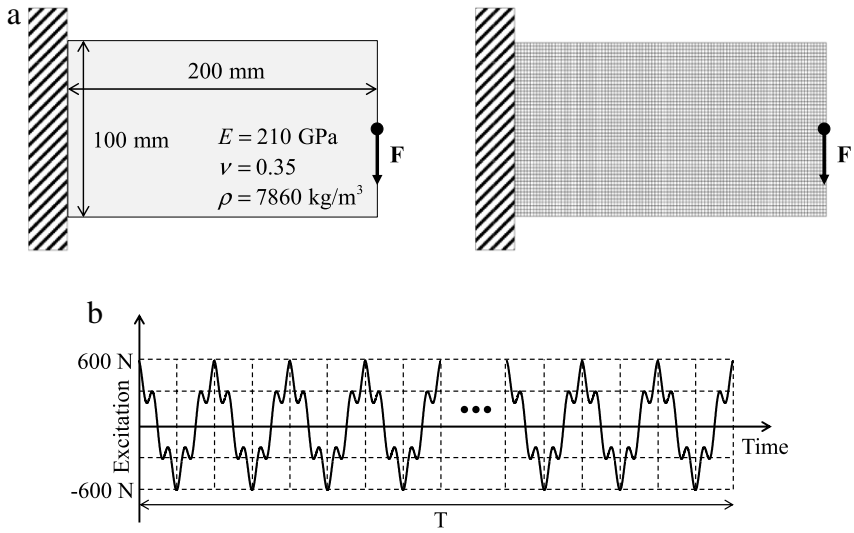

Fig. 8. An example of the singularity of accumulated damage. (a) An analysis domain and (b) the applied load ($F = F_1 e^{i\omega_1 t} + F_2 e^{i\omega_2 t}$, $F_1 = 450$ N, $\omega_1 = 2\pi$ (rad/s), $F_2 = 150$ N, $\omega_2 = 10\pi$ (rad/s), $T = 100$ s).

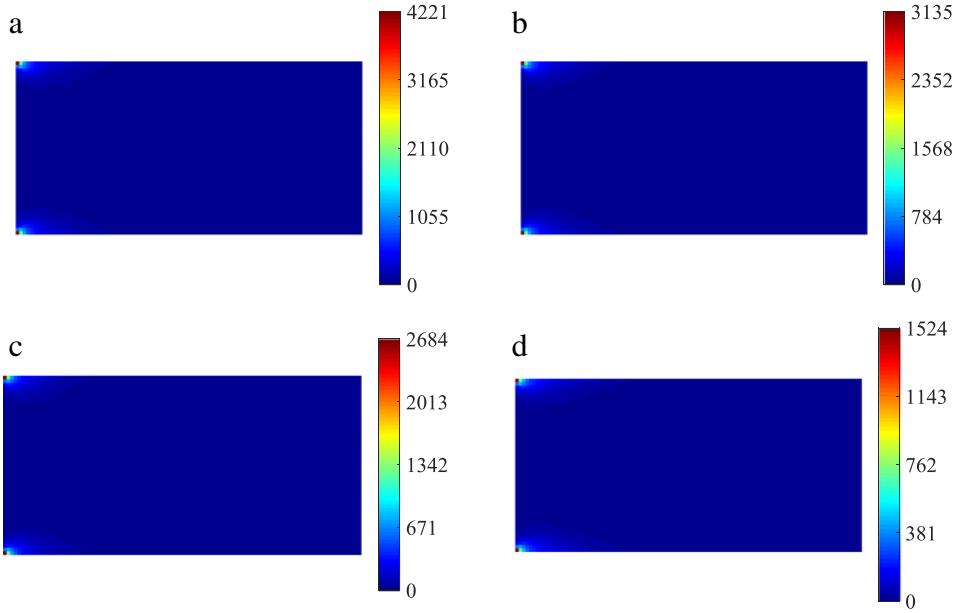

Fig. 9. Contours of the accumulated damage (density = 0.5): (a) Narrow band solution, (b) Wirsching and Light method, (c) Ortiz and Chen method and (d) Dirlik method.

where the accumulated damage, the total number of stress blocks, the number of actual loading cycles, and the number of loading cycles to failure under the ith stress are denoted by D, kn, n_i, and N_i, respectively. Note that Miner's rule assumes the applied loads cause purely alternating stresses with zeros for average stress values. For the ith-stress S_i, the number of loading cycles to failure, N_i, is computed by the S–N curve (Fig. 2).

$$NS^m = C \tag{2}$$

where C and m are the constants determined by the material used. The subscript, i, is intentionally omitted in N and S. The stress amplitude and the number of repeated stresses are denoted by S and N, respectively.

Despite a straightforward application of the S–N curve, it can be applied only to mechanical loads whose time histories are provided a priori and whose profiles are relatively simple or countable. With stochastic or long-span loads across decades, the application of the S–N curve becomes almost impossible, and other measures must be used for fatigue analysis. For example, in the offshore oil industry, the requirement for a rapid fatigue analysis method based on the frequency domain became apparent in designing large jacket platforms because fatigue failures had to be prevented. But fatigue analysis in

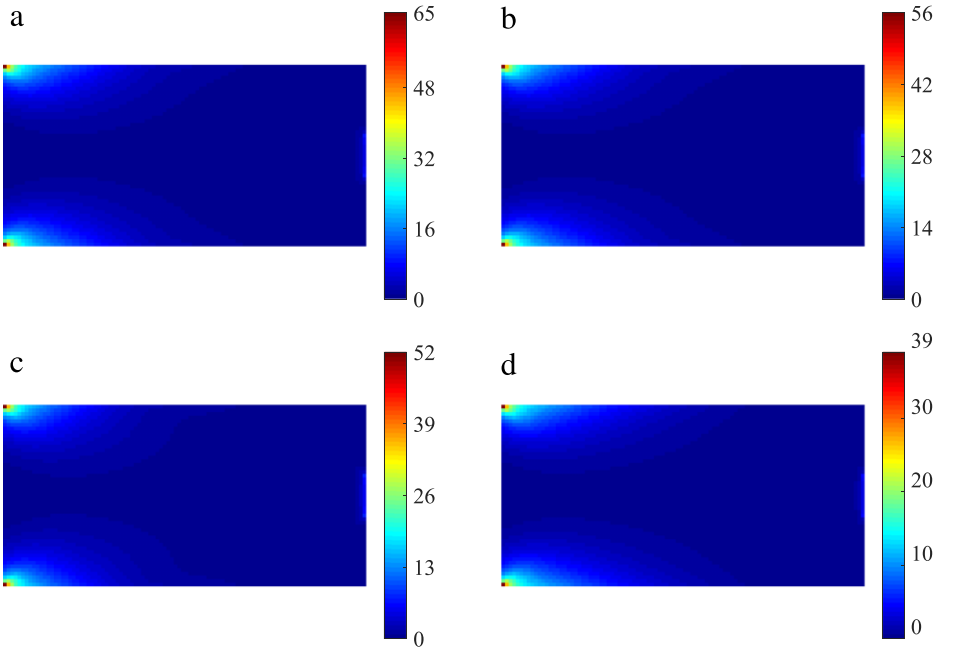

Fig. 10. Contours of the scaled accumulated damage from Fig. 9: (a) Narrow band solution, (b) Wirsching and Light method, (c) Ortiz and Chen method and (d) Dirlik method ($SF = 2$ and density $= 0.5$).

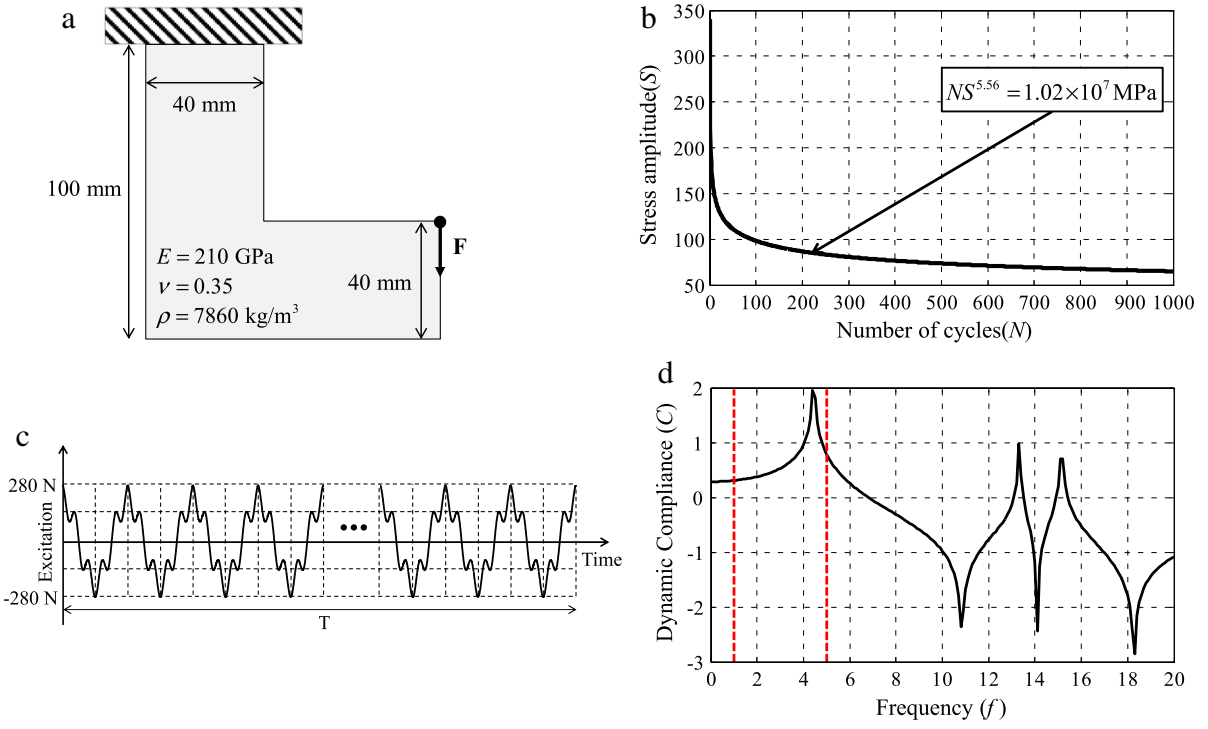

Fig. 11. L-shaped bracket problem. (a) The geometry and the load (the excited load was distributed on the six nodes on the tip of the right edge; the total number of elements in the design domain is 5000), (b) the S–N curve (C : 1.02×10^7 MPa and m: 5.56), (c) a mechanical load ($F = F_1 e^{i\omega_1 t} + F_2 e^{i\omega_2 t}$, F_1 : 135 N, $\omega_1 = 2\pi$, F_2 : 45 N, $\omega_2 = 10\pi$, $T = 100$ s), and (d) the frequency response function of dynamic compliance with the uniform design variables (density $= 1$).

the time domain becomes expensive because of the large number of degrees of freedom in FE models and the high number of possible load combinations, which makes the speedy calculation of a frequency domain analysis attractive. In connection with the S–N curve, one possible approach could be to use Miner's rule after analyzing load history in the frequency domain

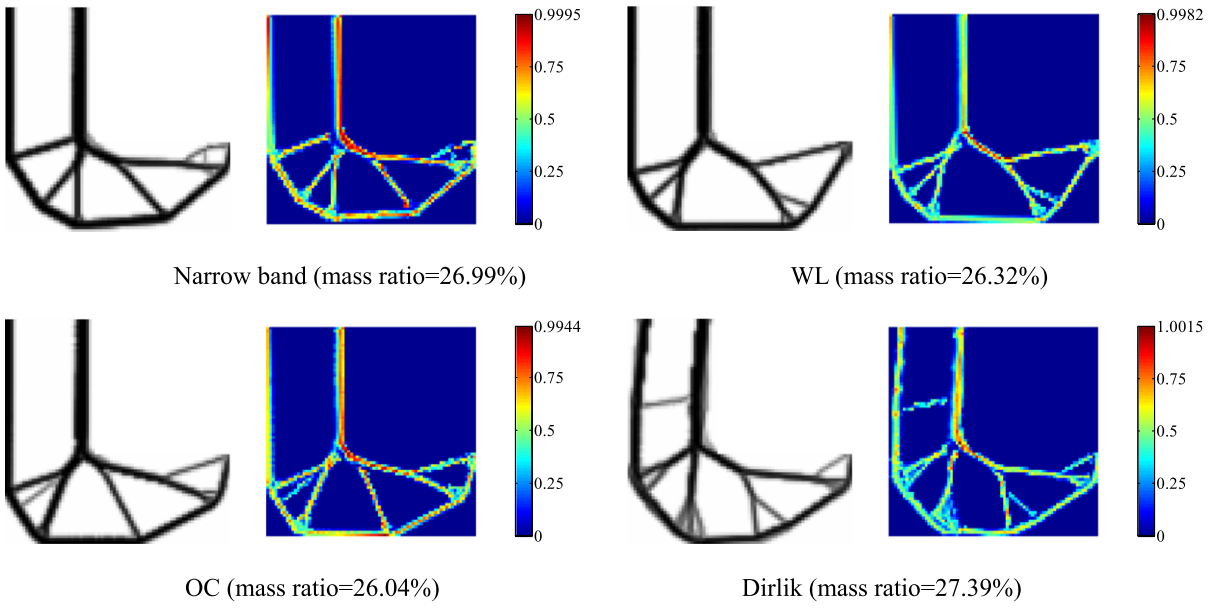

Fig. 12. Optimal layouts considering the fatigue constraint ($SF = 1.0$, WL = Wirsching and Light, OC = Ortiz and Chen).

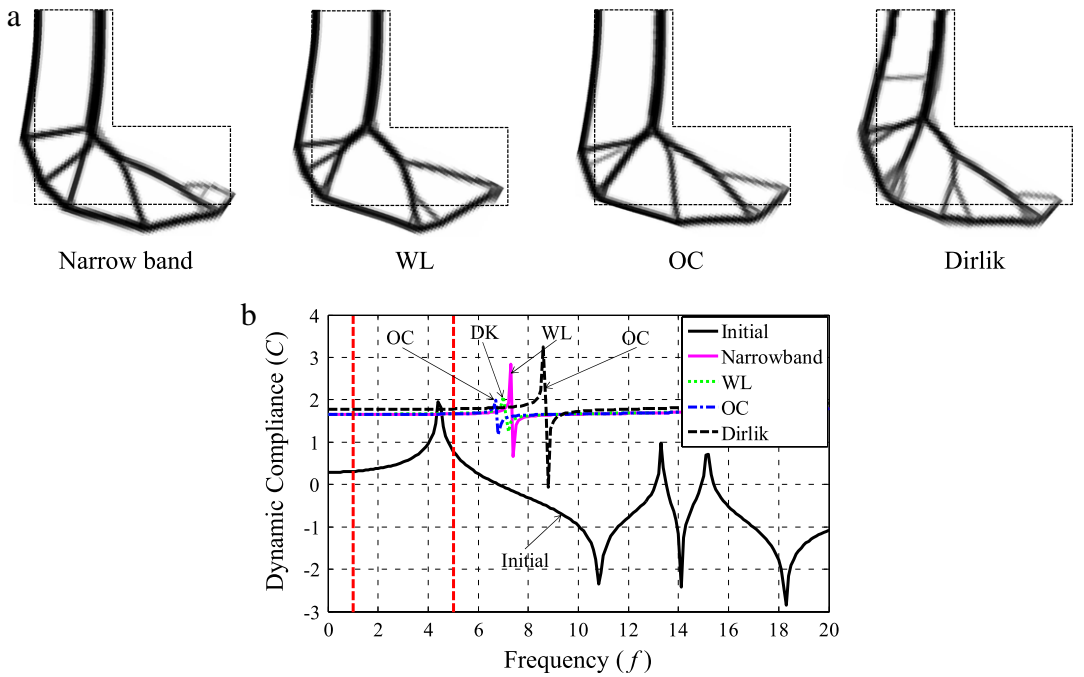

Fig. 13. Deformed shape and FRF (frequency response function): (a) the deformation of the optimal layouts ($SF = 1.0$, WL = Wirsching and Light, OC = Ortiz and Chen) and (b) the FRFs of the results. (Initial curve is Fig. 11(d).)

as follows:

$$D = \sum_{i=1}^{kn} \frac{n_i}{N_i} = \frac{E_p T}{C} \int_0^{\infty} S^m p(S)\, dS \tag{3}$$

where the expected rates of load peaks, the excited stress range, and the probability density function are denoted by E_p, S, and $p(S)$, respectively. The total period is denoted by T. In Eq. (3), the approximate rates of load peaks, E_p, can be indirectly

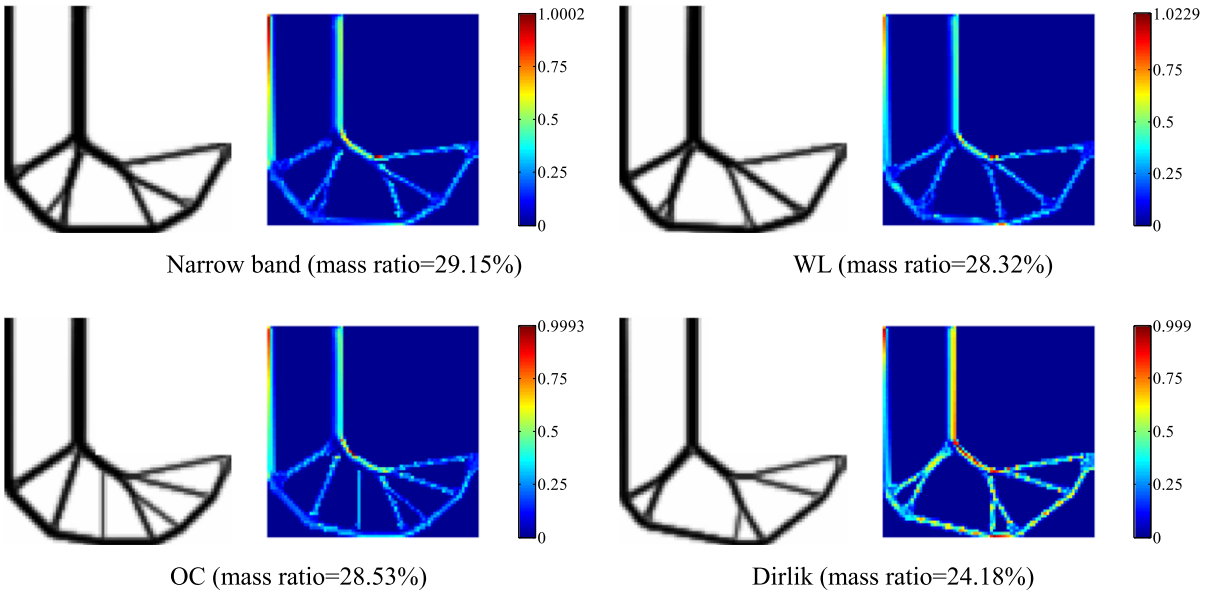

Fig. 14. Optimal layouts considering the fatigue constraint ($SF = 2$, WL = Wirsching and Light, OC = Ortiz and Chen).

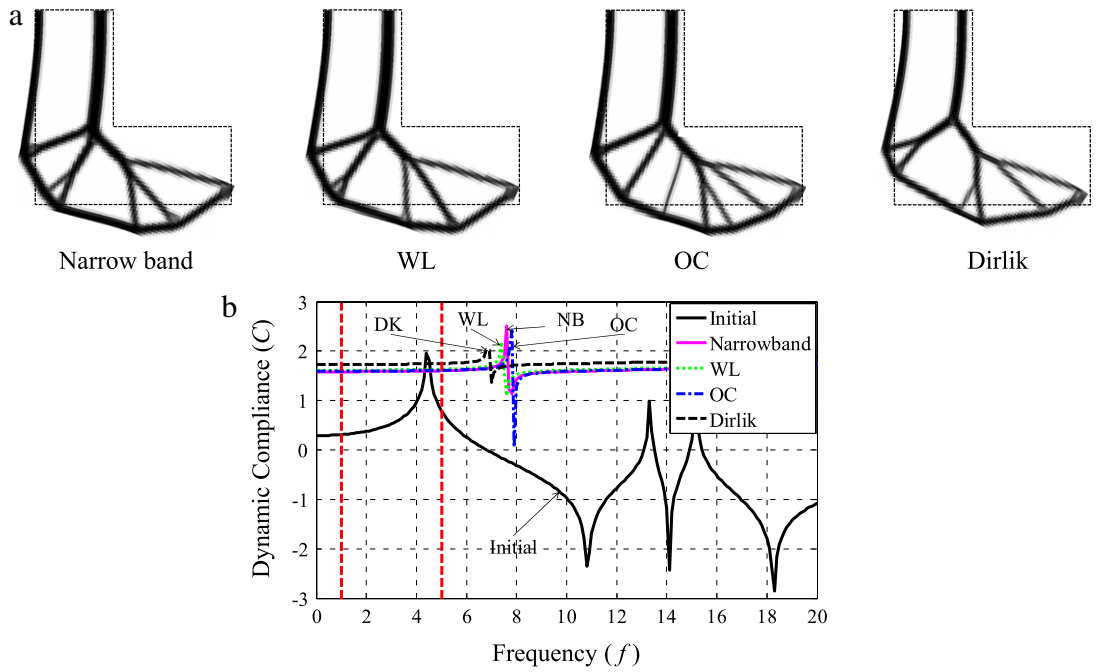

Fig. 15. Deformed shape and FRF (frequency response function): (a) the deformation of the optimal layouts ($SF = 2.0$, WL = Wirsching and Light, OC = Ortiz and Chen) and (b) the FRFs of the results. (Initial curve is Fig. 11(d).)

computed by:

$$E_p = \sqrt{\frac{m_4}{m_2}}, \qquad E_{0^+} = \sqrt{\frac{m_2}{m_0}} \tag{4}$$

where E_{0^+} is the approximate rate of zero up-crossing. The nth moment of a one-sided PSD function of alternating stress is denoted by m_n. Simply, the approximated numbers of load peaks and the numbers of zero up-crossings per second in the case of a random force in Fig. 3 are E_p and E_{0^+}, respectively.

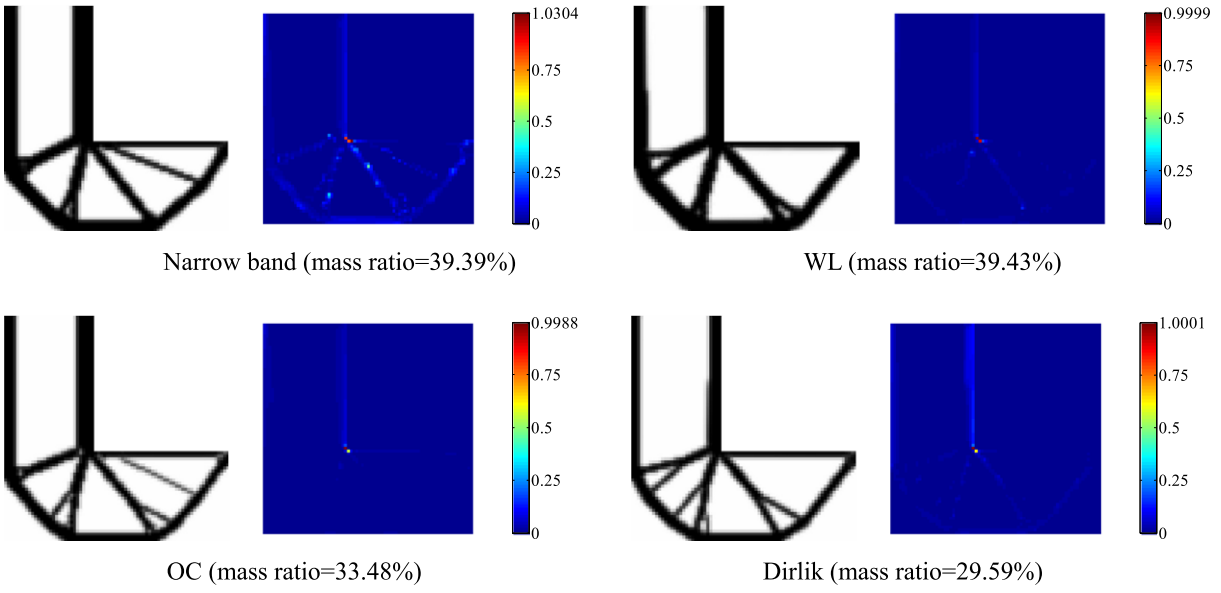

Fig. 16. Optimal layouts considering the fatigue constraint ($SF = 5$, WL = Wirsching and Light, OC = Ortiz and Chen).

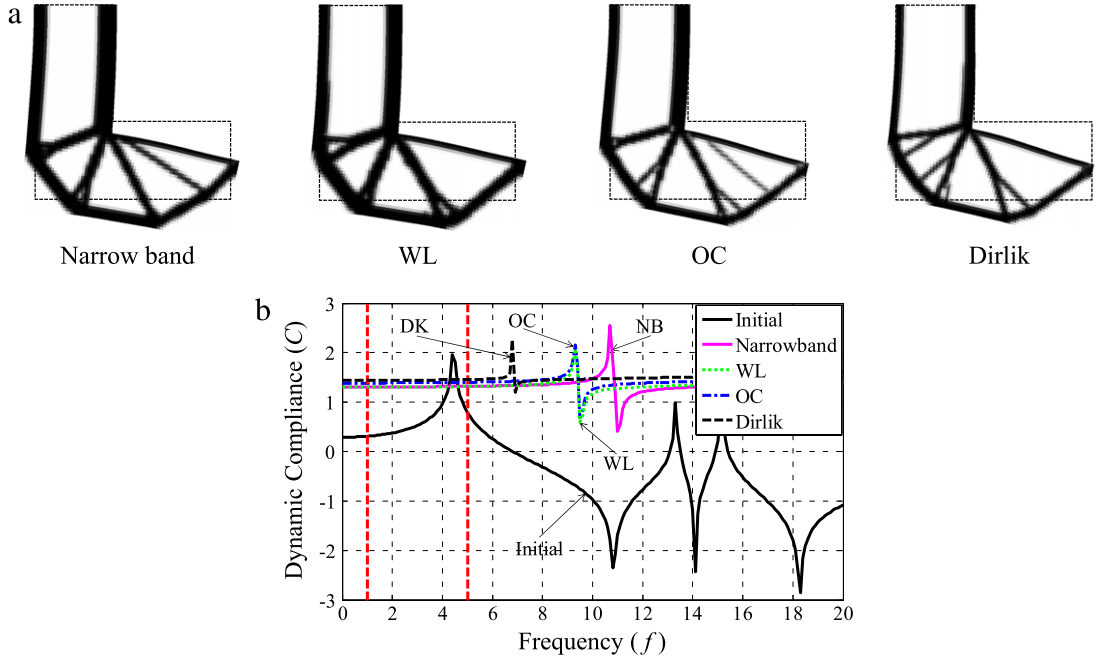

Fig. 17. Deformed shape and FRF (frequency response function): (a) the deformation of the optimal layouts ($SF = 5.0$, WL = Wirsching and Light, OC = Ortiz and Chen) and (b) the FRFs of the results. (Initial curve is Fig. 11(d).)

The nth moment of the PSD in Fig. 4 is defined as follows:

$$m_n = \int_0^\infty f^n W(f) df \tag{5}$$

where W is the power spectral density function for random stress.

As a random mechanical load can be presented in PDF form, it is possible to evaluate the damage for random mechanical load in the frequency domain. Fig. 5 shows an example PDF.

Because the results of a frequency response analysis of a general random mechanical load show multi-frequency components, it is not easy to integrate the integrals in Eqs. (3) and (5). Many approximate methods have been developed [4,9] and can be categorized depending on the region size of the frequency components in a random load, i.e., narrow frequency

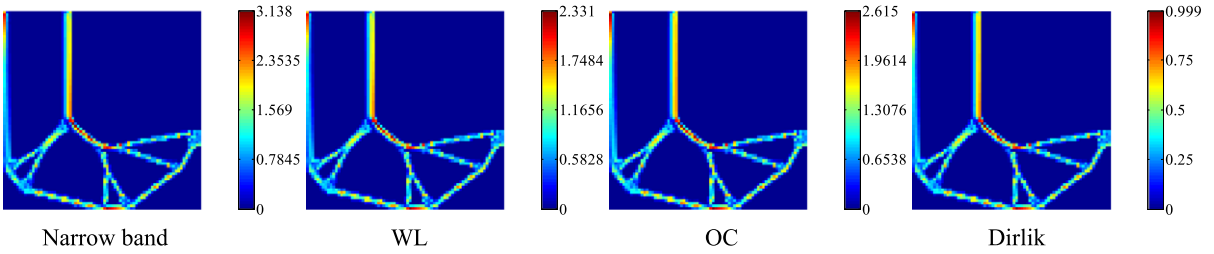

Fig. 18. Comparison of the fatigue damage of the design generated using Dirlik method as calculated by all four fatigue assessment methods ($SF = 2$, WL = Wirsching and Light, OC = Ortiz and Chen).

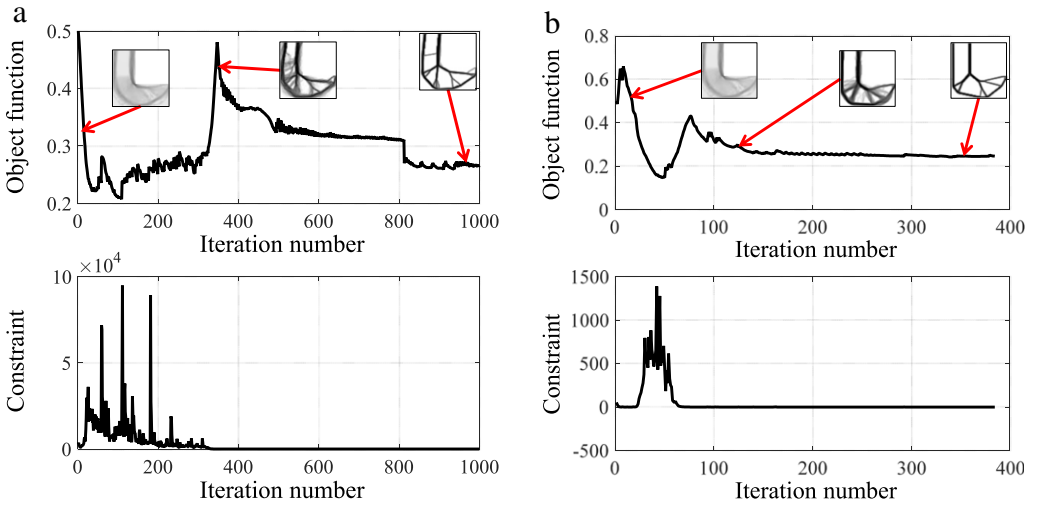

Fig. 19. Optimization histories of the designs by the Dirlik method: (a) $SF = 1$ and (b) $SF = 2$.

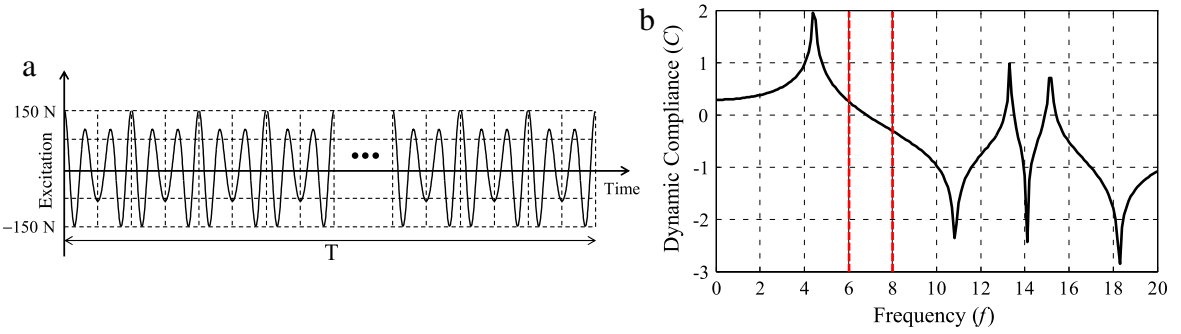

Fig. 20. Another mechanical load. (a) A high frequency mechanical load ($F = F_1 e^{i\omega_1 t} + F_2 e^{i\omega_2 t}$, F_1 : 112.5 N, $\omega_1 = 12\pi$, F_2 : 37.5 N, $\omega_2 = 16\pi$, $T = 100$ s) and (b) the frequency response function of dynamic compliance with the uniform design variables (density = 1).

region or wide frequency region. For a random load with a narrow frequency region, the narrow band solution is available. For a random load with a wide frequency region, the Wirsching and Light method, the Ortiz and Chen method, and Dirlik method have been proposed [3–9]. These approaches adopt different PDFs.

Narrow band solution

In the narrow band solution, the simplest PDF in Eq. (6) is used.

$$p(S) = \frac{S}{4m_0} e^{\frac{-S^2}{8m_0}} \tag{6}$$

where S is the stress amplitude and m_0 is the 0th moment. Its peak counting example is shown in Fig. 6. Because the PDF function is simple, its computation is relatively easy and straightforward. One of the pitfalls of this method is that as it always

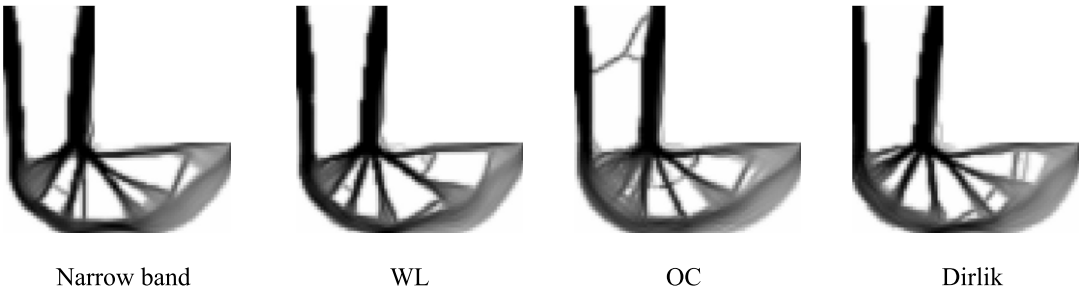

Fig. 21. Designs with no scaling factor.

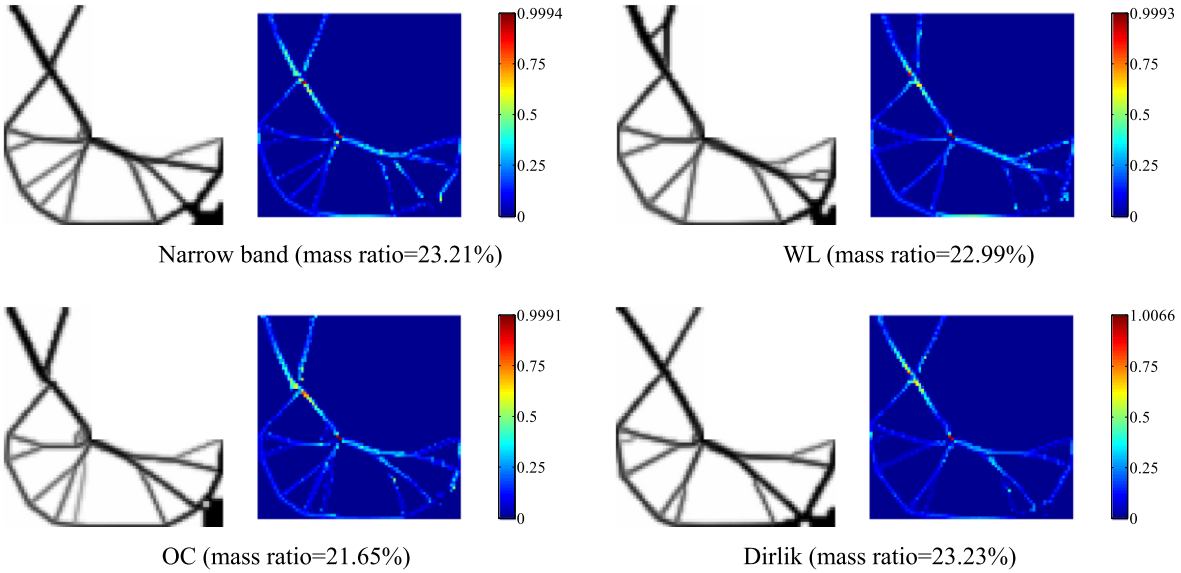

Fig. 22. Optimal layouts considering the fatigue constraint for the mechanical load in Fig. 20. ($SF = 2$, WL = Wirsching and Light, OC = Ortiz and Chen).

assumes that one positive peak follows one negative peak with the same magnitude for a positive valley for one cycle, as shown in Fig. 6(a); positive valleys and negative floors are ignored in a wide frequency range in Fig. 6(b).

For example, consider the mechanical load in Fig. 7(a), which is the combination of a low frequency load (1 Hz) and a high frequency load (10 Hz). With the narrow band solution, the mechanical load is approximated as shown in Fig. 7(b) and (c). Therefore, the narrow band solution method becomes a conservative measure in fatigue design.

The Wirsching–Light method and the Ortiz–Chen method

As explained above, the narrow band solution is a conservative or incorrect measure for a mechanical load with a wide frequency range. To consider fatigue in a wide frequency range, some alternative methods, such as the Wirsching and Light method [5] and the Ortiz and Chen method [6], have been proposed. In the Wirsching and Light method, the accumulated damage can be calculated as follows:

$$D_{WL} = \zeta_W D_{NB} \tag{7}$$

$$\zeta_W = a_W + [1 - a_W]\,(1 - \lambda)^{b_W}, \quad \lambda = \frac{m_2}{\sqrt{m_0 m_4}} \tag{8}$$

$$a_W = 0.926 - 0.033m, \qquad b_W = 1.587m - 2.323 \tag{9}$$

where D_{WL} is the accumulated damage approximated by the Wirsching and Light method. The accumulated damage calculated by the narrow band solution is denoted by D_{NB}. The m is the exponent value in Eq. (2).

Similar to the Wirsching and Light method, the Ortiz and Chen method calculates the accumulated damage as follows:

$$D_{OC} = \zeta_O D_{NB} \tag{10}$$

$$\zeta_O = \frac{1}{\kappa}\sqrt{\frac{m_2 m_l}{m_0 m_{l+2}}}, \quad l = \frac{2.0}{m}, \; \kappa = \frac{m_2}{\sqrt{m_0 m_4}} \tag{11}$$

where the accumulated damage defined by the Ortiz and Chen method is D_{OC}.

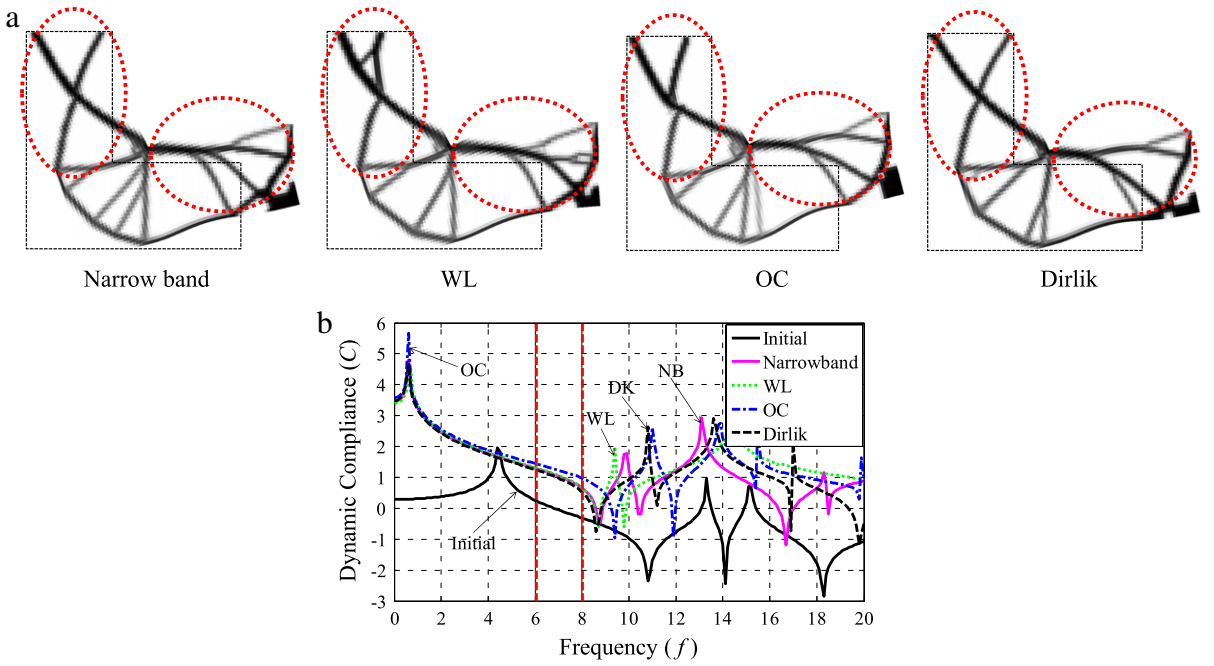

Fig. 23. Deformed shape and FRF (frequency response function): (a) the deformation of the optimal layouts ($SF = 2.0$, WL = Wirsching and Light, OC = Ortiz and Chen) and (b) the FRFs of the results. (Initial curve is Fig. 20 (b).)

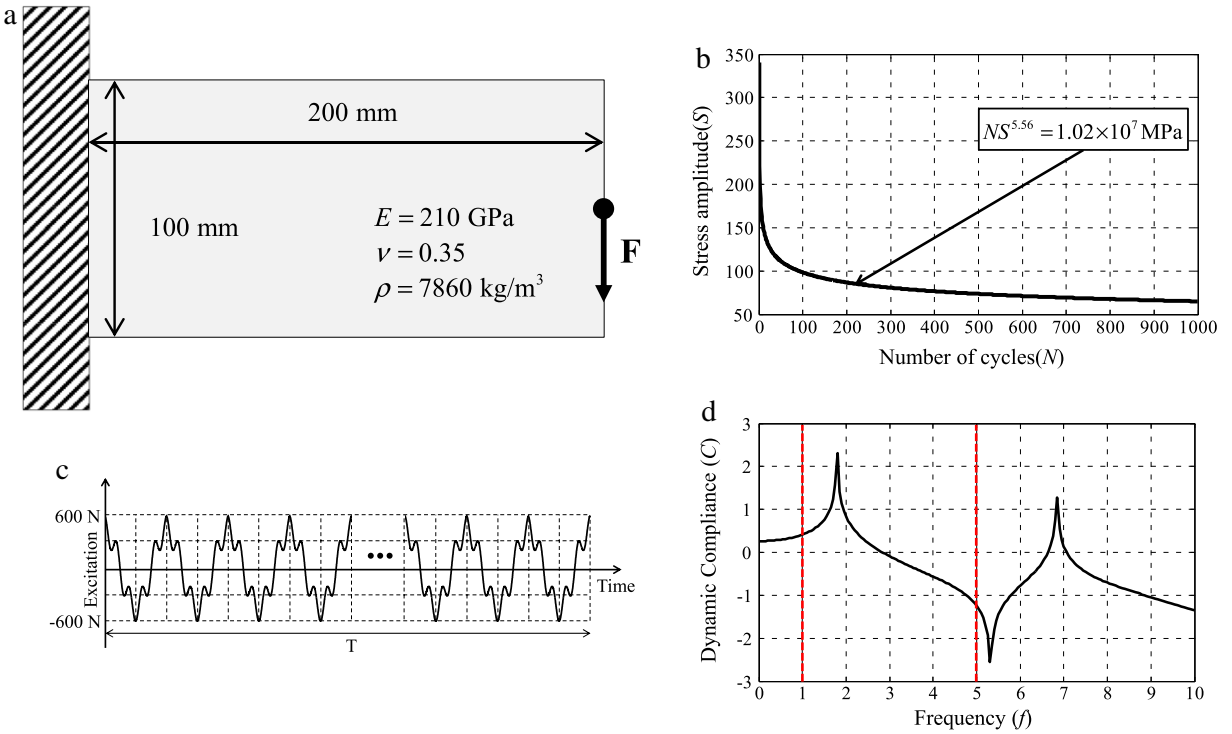

Fig. 24. Cantilever beam problem. (a) The geometry and the load (the excited load is distributed on the eleven nodes in the center of the right edge; the total number of elements in the design domain is 5000, and the number of reinforcement elements is 600), (b) the S–N curve ($C : 1.02 \times 10^7$ MPa and $m : 5.56$), (c) a mechanical load ($F = F_1 e^{i\omega_1 t} + F_2 e^{i\omega_2 t}$, $F_1 : 450$ N, $\omega_1 = 2\pi$, $F_2 : 150$ N, $\omega_2 = 10\pi$, $T = 100$ s) and (d) the frequency response function of dynamic compliance with the uniform design variables (density = 1).

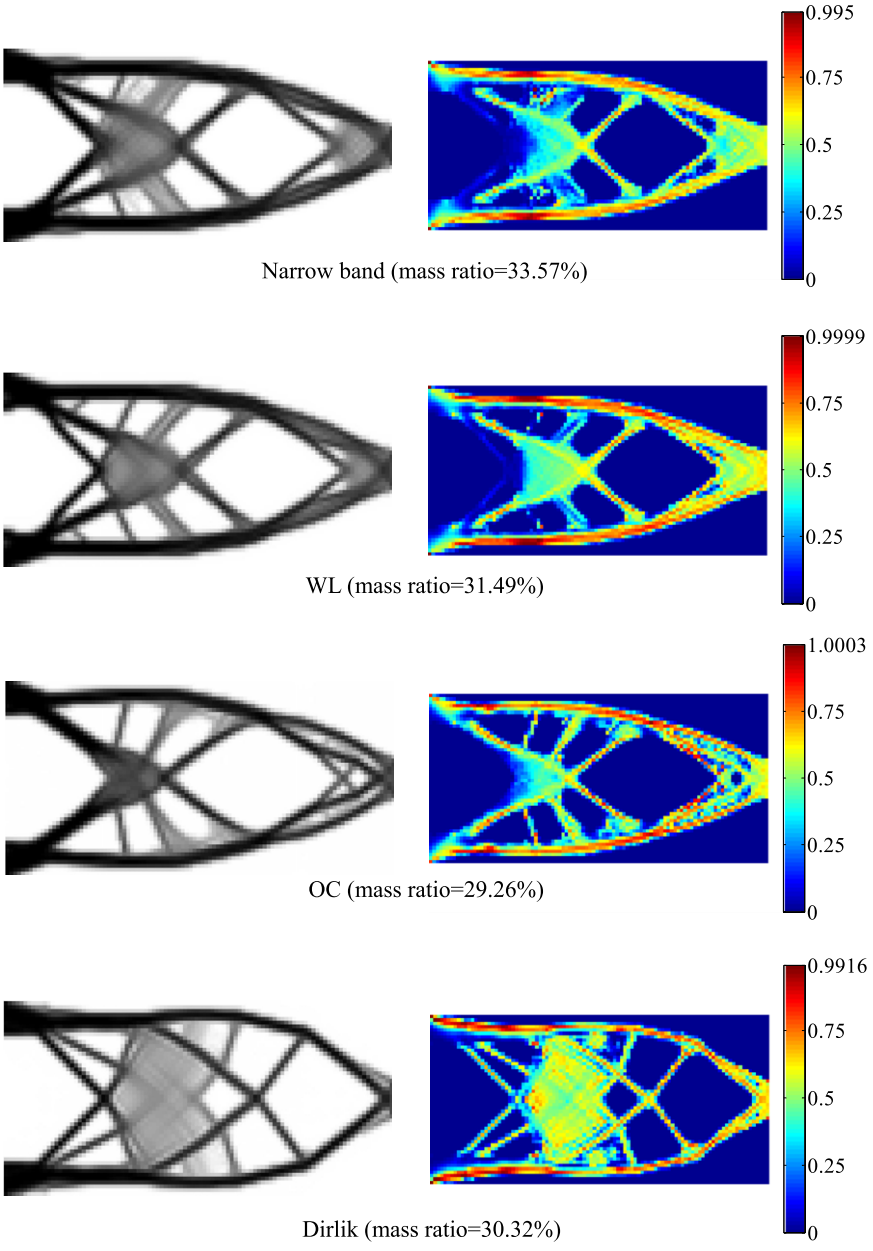

Fig. 25. Optimal layouts considering the fatigue constraint ($SF = 1.0$, WL = Wirsching and Light, OC = Ortiz and Chen).

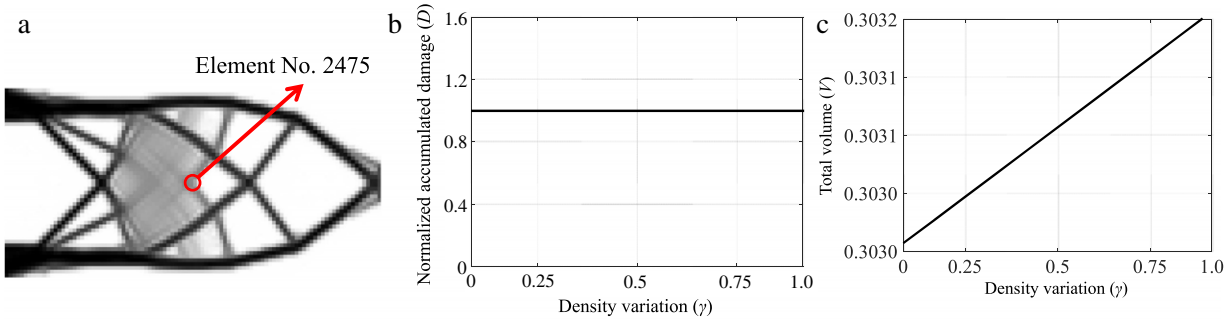

Fig. 26. The effect of the gray element (2475th element): (a) location of the 2475th element, (b) change of the normalized accumulated damage and (c) change of the total volume.

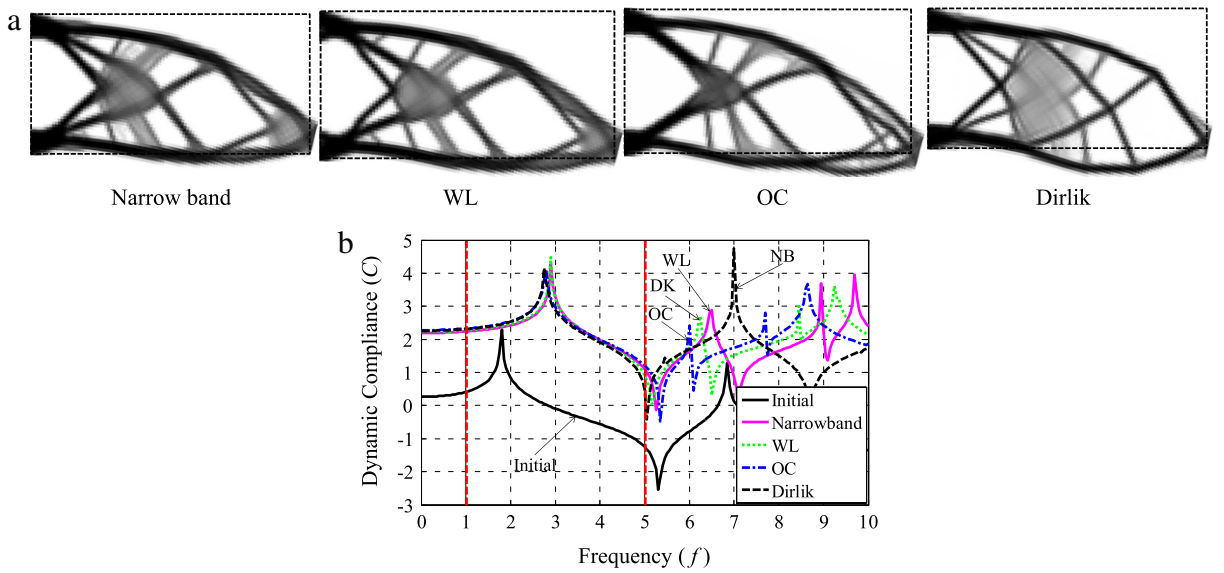

Fig. 27. Deformed shape and FRF (frequency response function): (a) the deformation of the optimal layouts ($SF = 1.0$, WL = Wirsching and Light, OC = Ortiz and Chen) and (b) the FRFs of the results. (Initial curve is Fig. 24(d).)

Dirlik method

The Wirsching and Light method and the Ortiz and Chen method are experimental formulations based on the narrow band solution used to overcome its limitations. However a more accurate method is presented by selecting another PDF, as shown in Eq. (12).

$$p(S) = \frac{1}{2\sqrt{m_0}}\left[\frac{D_1}{Q}e^{\frac{-Z}{Q}} + \frac{D_2 Z}{R^2}e^{\frac{-Z^2}{2R^2}} + D_3 e^{\frac{-Z^2}{2}}\right] \tag{12}$$

$$Z = \frac{S}{2\sqrt{m_0}}, \qquad \kappa = \frac{m_2}{\sqrt{m_0 m_4}}, \qquad X = \frac{m_1}{m_0}\sqrt{\frac{m_2}{m_4}}, \qquad Q = \frac{1.25(\kappa - D_3 - D_2 R)}{D_1}$$

$$D_1 = \frac{2\left(X - \kappa^2\right)}{1+\kappa^2}, \qquad D_2 = \frac{1 - \kappa - D_1 + D_1^2}{1 - R}, \qquad D_3 = D_1 - D_2, \qquad R = \frac{\kappa - X - D_1^2}{1 - \kappa - D_1 + D_1^2}$$

where the involved parameters are Z, κ, X, Q, D_1, D_2, D_3, and R. With Dirlik method, *a more accurate prediction is possible; see* [4,7–9] *for more details.*

2.2. Finite element analysis

For TO considering fatigue, this research uses the finite element procedure. Because we need to consider the harmonic responses of a structure, we adopt the following harmonic finite element procedure.

$$\left(\mathbf{K} - \omega^2 \mathbf{M}\right)\mathbf{U} = \mathbf{K}_D \mathbf{U} = \mathbf{F} \tag{13}$$

where the mass matrix, the stiffness matrix, and the dynamic stiffness matrix are denoted by K, M, and K_D, respectively. The displacement and the force vectors are U and F, respectively. The angular frequency is ω. The stiffness matrix and the mass matrix are constructed by following standard FE procedures.

$$\mathbf{K} = \sum_{e=1}^{NE} \mathbf{k}_e \quad \text{and} \quad \mathbf{k}_e = \int_{\Omega_e} \mathbf{B}^{\mathrm{T}} \mathbf{C}_e \mathbf{B} dv \quad (\Omega_e : \text{the } e\text{th element domain}) \tag{14}$$

$$\mathbf{M} = \sum_{e=1}^{NE} \mathbf{m}_e \quad \text{and} \quad \mathbf{m}_e = \int_{\Omega_e} \rho \mathbf{N}^{\mathrm{T}} \mathbf{N} dv \quad (\rho : \text{the nominal density}) \tag{15}$$

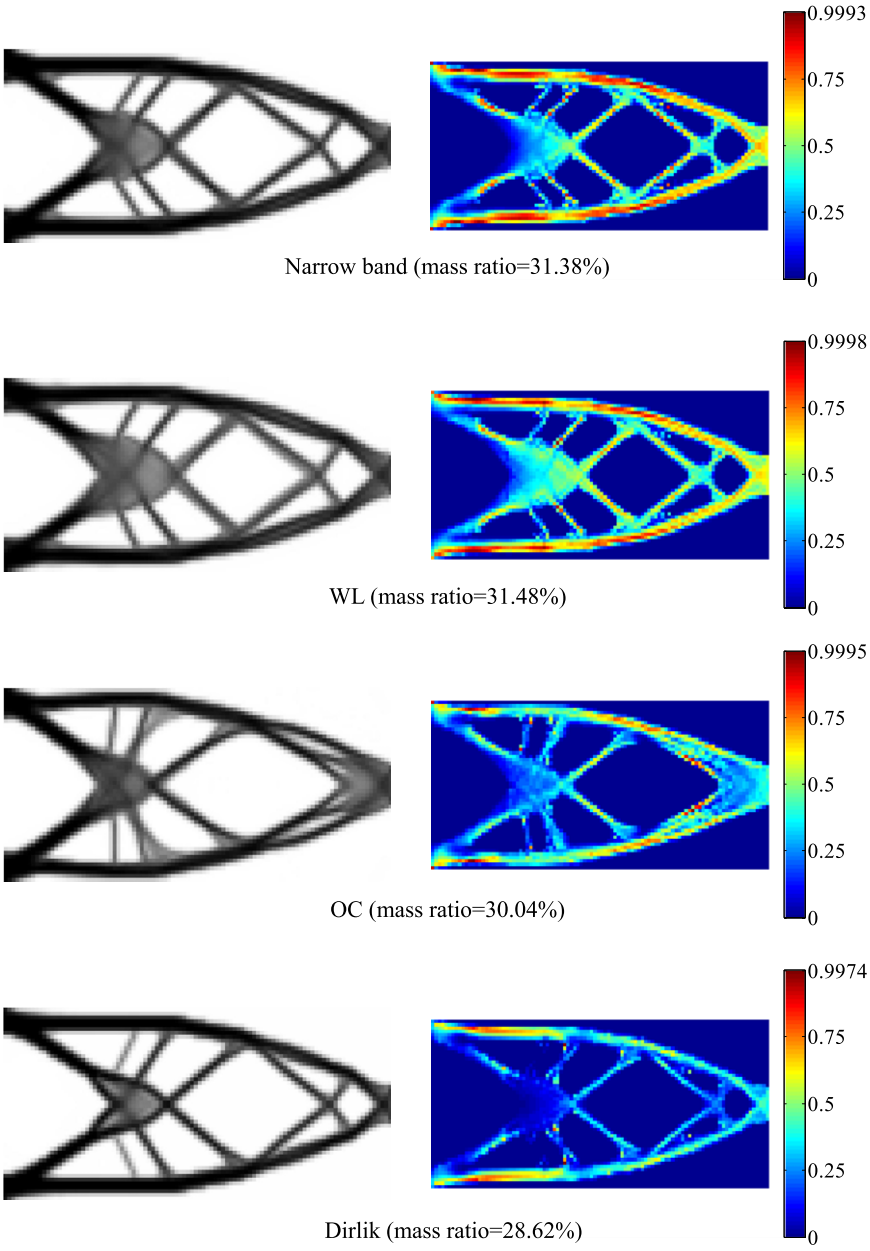

Fig. 28. Optimal layouts considering the fatigue constraint ($SF = 2$, WL = Wirsching and Light, OC = Ortiz and Chen).

where the constitutive matrix and the strain–displacement matrix are $\mathbf{C}_e$ and $\mathbf{B}$, respectively. The shape function is denoted by $\mathbf{N}$. The number of finite elements is NE.

3. Topology optimization formulation for the fatigue constraint in the frequency domain

3.1. Optimization formulation and material interpolation

Optimization formulation

This section presents a new TO formulation based on a fatigue life method in the frequency domain. The objective is an extension of the stress-based TO problem minimizing the volume subject to local static stress constraints. Due to some numerical difficulties and issues, many innovative approaches, such as the density filter, the qp-relaxation method, the p-norm approach, and regional constraints, have been proposed. Initiated by that research, the following optimization

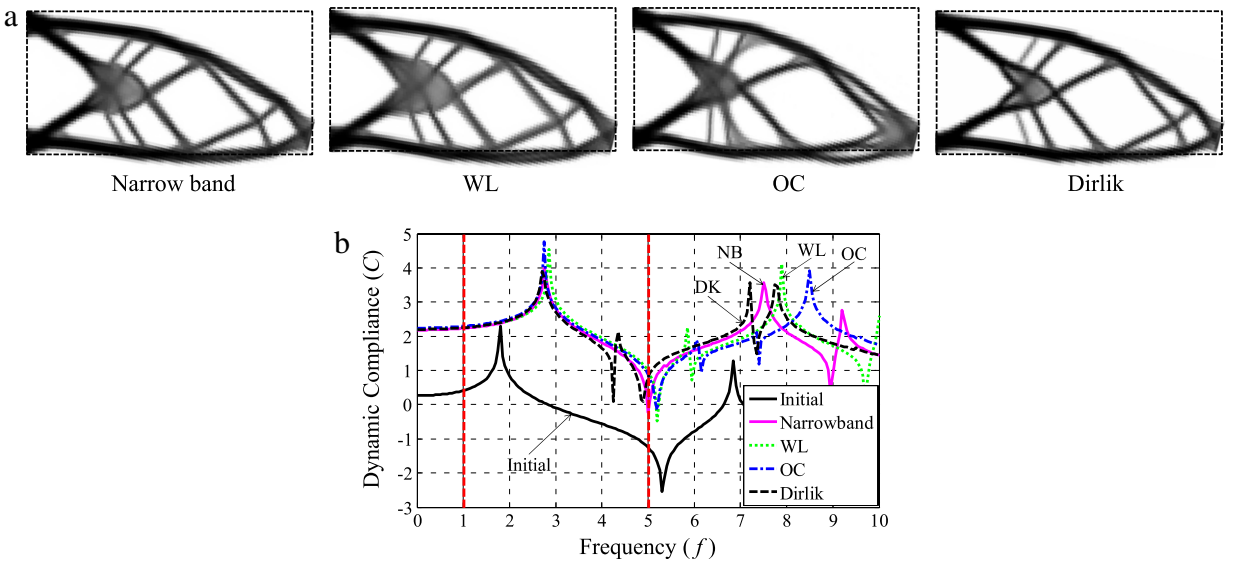

Fig. 29. Deformed shape and FRF (frequency response function): (a) the deformation of the optimal layouts ($SF = 2.0$, WL = Wirsching and Light, OC = Ortiz and Chen) and (b) the FRFs of the results. (Initial curve is Fig. 24(d).)

problem is considered here.

$$\begin{aligned} &\underset{\tilde{\gamma}}{\text{Minimize}} \quad V(\tilde{\boldsymbol{\gamma}}) = \sum_{e=1}^{NE} \tilde{\gamma}_e v_e \ (\tilde{\boldsymbol{\gamma}} : \text{filtered density}) \\ &\text{Subject to} \quad \langle D_{\max} \rangle \leq 1 \\ &\tilde{\boldsymbol{\gamma}} = \Xi \ (\boldsymbol{\gamma}) \ \text{with the density filter } \Xi \end{aligned} \tag{16}$$

$$\langle D_{\max} \rangle \equiv C^{iter} \left(\sum_{e}^{NE} D_e^p \tilde{\gamma}_e \right)^{\frac{1}{p}} \quad (e \in \Omega_e) \tag{17}$$

$$\langle D_{PN} \rangle \equiv \left(\sum_{e}^{NE} D_e^p \tilde{\gamma}_e \right)^{\frac{1}{p}} \quad (e \in \Omega_e) \tag{18}$$

$$C^{iter} = \alpha \frac{D_{\max}^{iter-1}}{\langle D_{PN} \rangle^{iter-1}} + (1-\alpha) C^{iter-1} \quad 0 < \alpha < 1 \tag{19}$$

where the eth design variable and the eth filtered design variable are denoted by γ_e and $\tilde{\gamma}_e$, respectively. The eth volume is v_e. The accumulated damage of the eth element is D_e. The value of the p-norm is denoted by p, and a positive value from 3 to 5 is used for p. The correction factor at the $iter$-th optimization iteration, the maximum accumulated damage value at the $iter$-th optimization iteration, and the damping factor are denoted by C^{iter}, $D_{\max}^{iter}$, and α, respectively.

Material interpolation for TO

Following the SIMP method, the constitutive matrix $\mathbf{C}_e$ is interpolated as:

$$\mathbf{C}_e = \gamma_e^{n_k} \mathbf{C}_0 \tag{20}$$

$$\text{Plane stress} : \ \mathbf{C}_0 = \frac{E_0}{1-\nu^2} \begin{bmatrix} 1 & \nu & 0 \\ \nu & 1 & 0 \\ 0 & 0 & \dfrac{1-\nu}{2} \end{bmatrix} \tag{21}$$

where the eth design variable is γ_e with the penalization n_k. Nominal Young's modulus and Poisson's ratio are denoted by E_0 and ν, respectively.

For TO, the stress at the eth element is evaluated as follows:

$$\boldsymbol{\sigma}_e = \mathbf{C}_{S,e} \mathbf{B} \mathbf{u}_e \tag{22}$$

$$\mathbf{C}_{S,e} = \gamma_e^{n_S} \mathbf{C}_0 \tag{23}$$

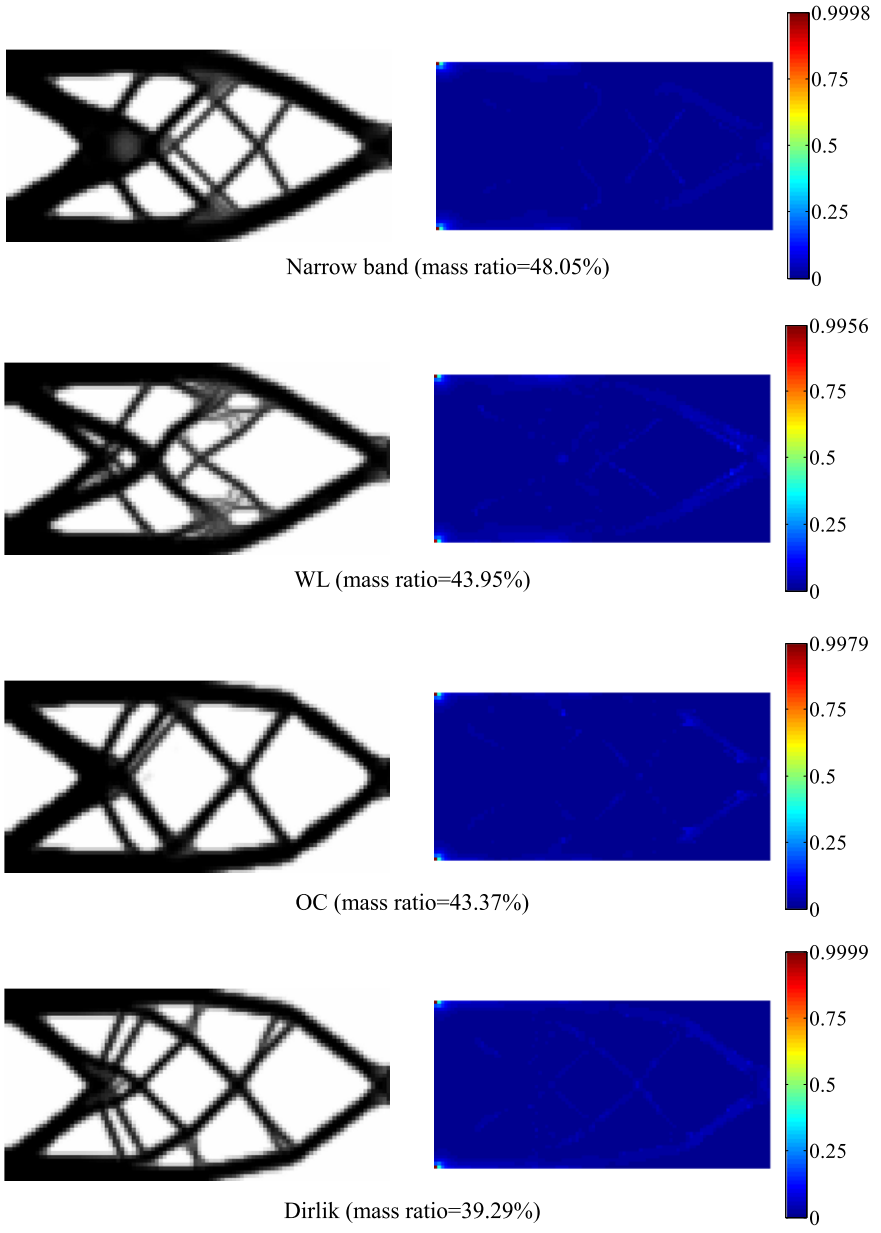

Fig. 30. Optimal layouts considering the fatigue constraint ($SF = 5$, WL = Wirsching and Light, OC = Ortiz and Chen).

where the stress and displacements of the eth element are denoted by $\boldsymbol{\sigma}_e$ and $\mathbf{u}_e$, respectively. The penalization parameter for the stress evaluation is n_s. Here it should be noticed that the above formulations adopt the inconsistent constitutive matrix $\mathbf{C}_{S,e}$ to overcome the singularity issue in the stress-based TO; see [17,21,26] for more details. The common penalty factors for n_k and n_s are 3 and 0.5, respectively. The mass matrix is interpolated and formulated as:

$$\mathbf{M} = \sum_{e=1}^{NE} \gamma_e^{n_m} \mathbf{m}_e \tag{24}$$

where the penalization parameter for the mass matrix is denoted by n_m. This penalization factor is set to a positive value higher than n_k to avoid the localized mode issue; see [16] for more details.

The constraint controlling issue

When we adopt the direct formulation for the accumulated damage in Eq. (18), the singularity of the constraint with respect to the design variable is observed; this singularity is not related to the stress singularity issue. To show this feature, the cantilever structure of Fig. 8 can be considered. With an even material distribution inside the rectangular design domain,

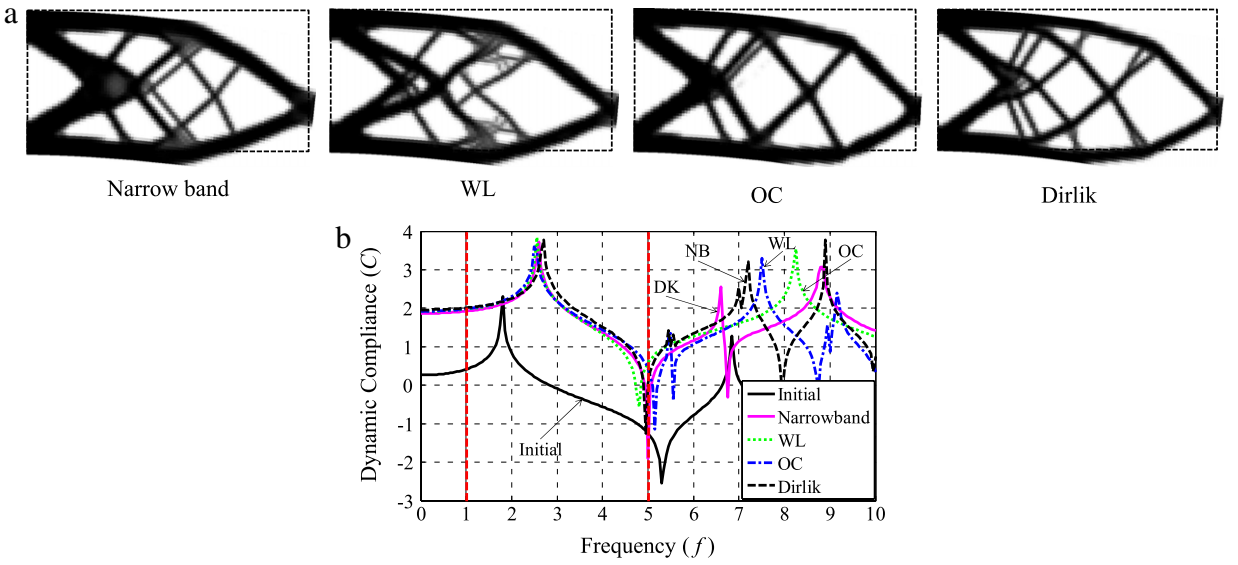

Fig. 31. Deformed shape and FRF (frequency response function): (a) the deformation of the optimal layouts ($SF = 5.0$, WL = Wirsching and Light, OC = Ortiz and Chen) and (b) the FRFs of the results. (Initial curve is Fig. 24(d).)

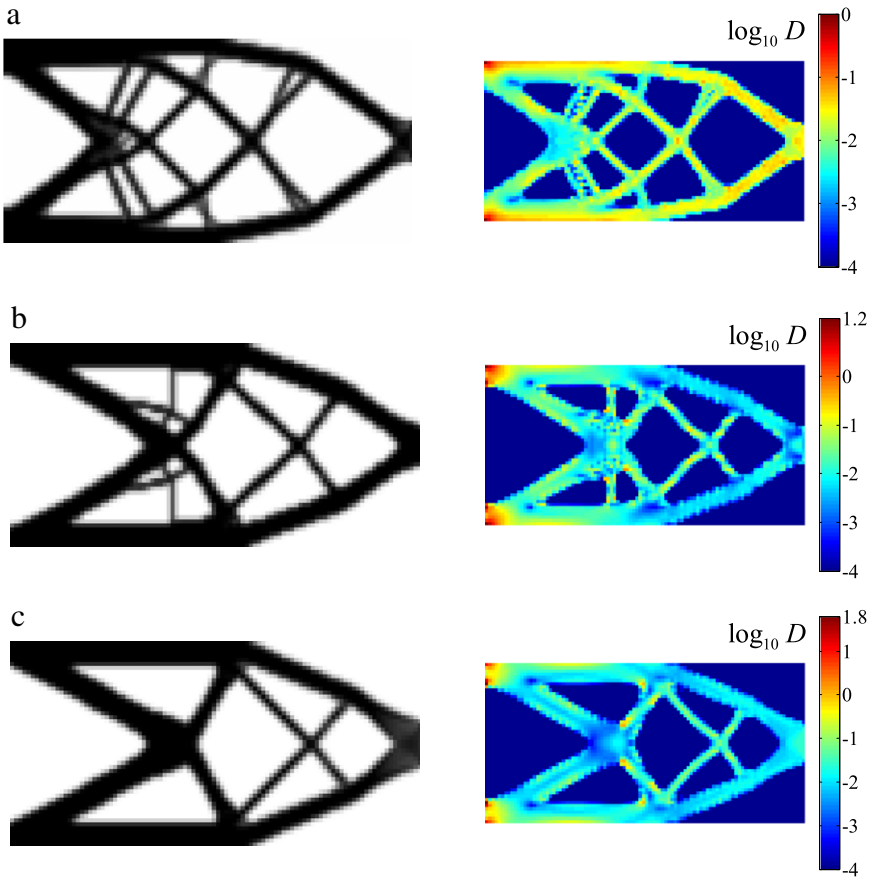

Fig. 32. Comparison with the compliance minimization problem (the damage plotted in the logarithm scale: $\log_{10} D$): (a) the optimized layout in Fig. 30(d) (Dirlik method) and the accumulated damage distribution (b) the layout minimizing the compliance subject to the mass constraint (Mass ratio = 40%) and the accumulated damage distribution and (c) the layout minimizing the dynamic compliance subject to the mass constraint (Mass ratio = 40%) and the accumulated damage distribution.

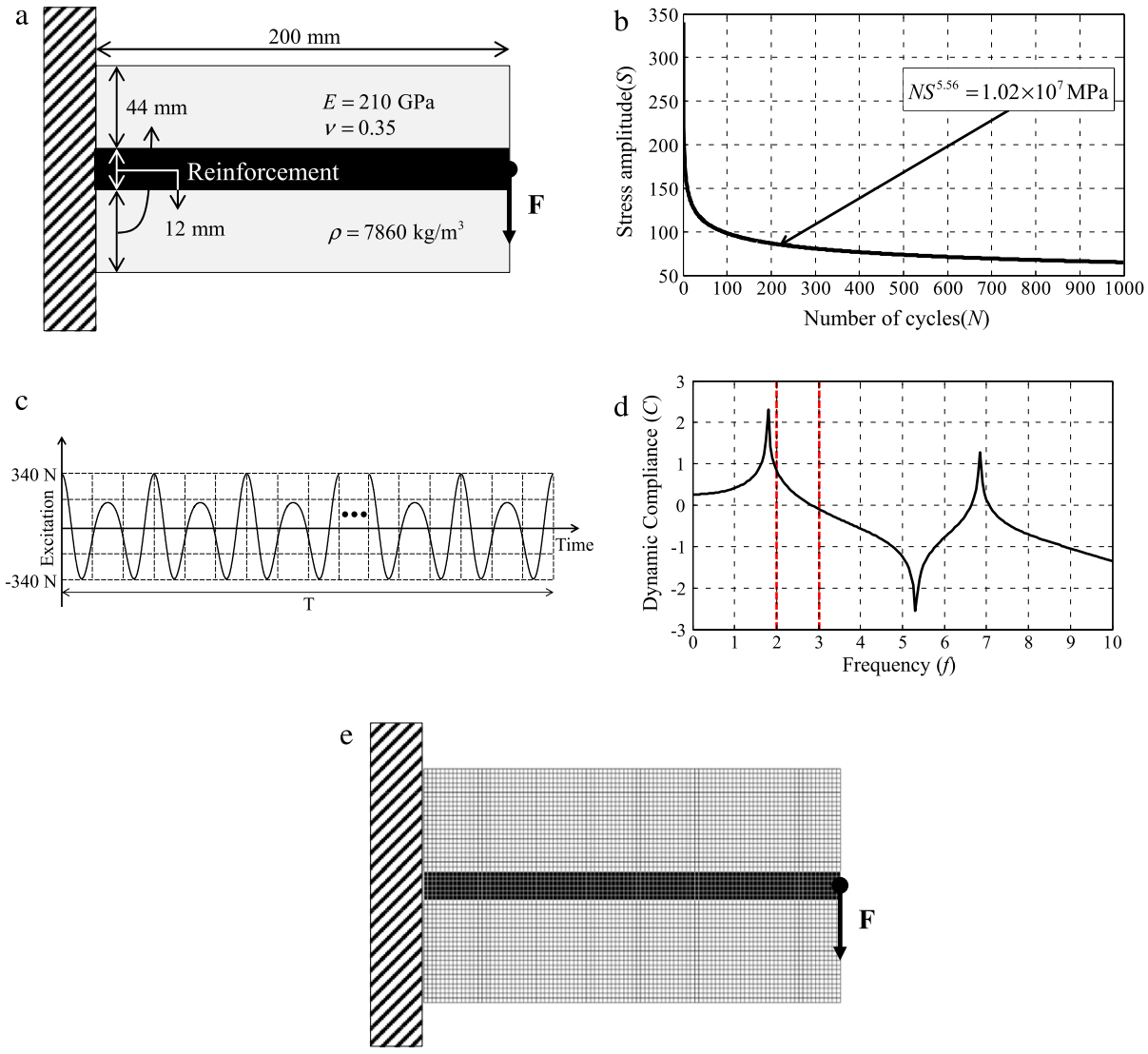

Fig. 33. Reinforced cantilever beam structure problem. (a) The geometry and the load (the excited load is distributed on the eleven nodes in the center of the right edge), (b) the S–N curve (C : 1.02×10^7 MPa and m: 5.56), (c) a mechanical load ($F = F_1 e^{i\omega_1 t} + F_2 e^{i\omega_2 t}$, F_1 : 170 N, $\omega_1 = 4\pi$, F_2 : 170 N, $\omega_2 = 6\pi$, $T = 1000$ s), (d) the frequency response function of dynamic compliance with the uniform design variables (density = 1), and (e) a finite element model of the design domain (total number of design domain elements is 5000, and the number of reinforcement elements is 600).

the accumulated damage calculated for the load in Fig. 8(b) by each method is plotted in Fig. 9. As shown, the two end corners at the clamped side show very high accumulated damage compared with the accumulated damage in other areas or to the finite elements. Depending on the numerical approach for a gradient-based optimizer to deal with this singularity, some different layouts can be obtained.

To prevent this singularity issue in analysis and design, we propose to use the following scaling factor, SF, of the accumulated damage at each finite element.

$$\tilde{D} = D^{\frac{1}{SF}} = \left(\sum_{i=1}^{kn} \frac{n_i}{N_i} \right)^{\frac{1}{SF}}. \tag{25}$$

The accumulated damage, D, is sensitive to small variations of the density variables. By taking the exponent $1/SF$ the singularity of D can be relaxed.

Fig. 10 shows the scaled accumulated damage of the original damage in Fig. 9. Fig. 10 shows the distribution of scaled accumulated damage with 1.5 of SF. As shown, the big differences in the magnitudes are reduced. The maximum gradient value of the accumulate damages is about 1524 in the unscaled case and the localization problem of the gradient of the accumulated damage is serious. However the maximum value is reduced as about 39 after applying the scale factor. So it

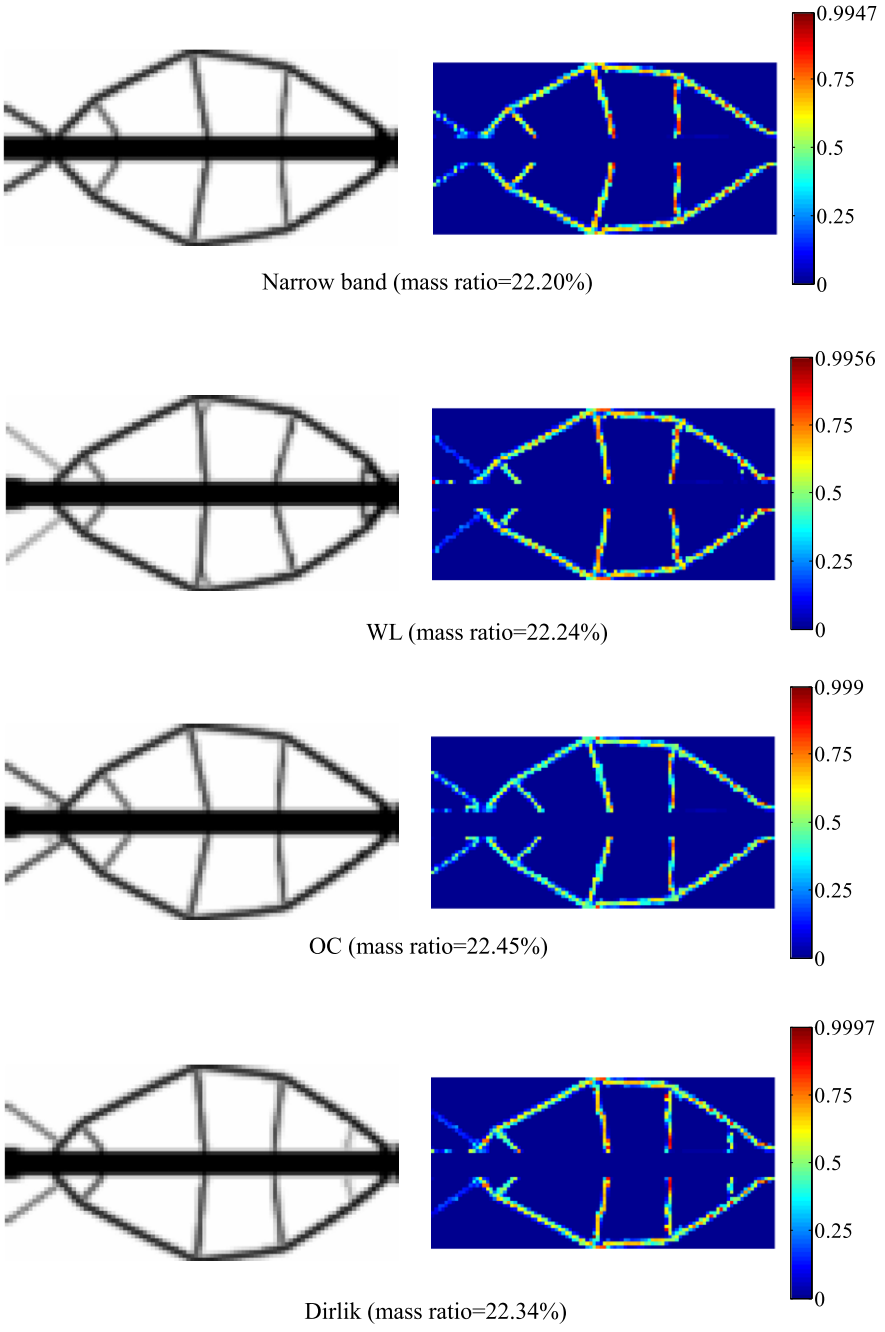

Fig. 34. Optimal layouts considering the fatigue constraint ($SF = 1.0$, WL = Wirsching and Light, OC = Ortiz and Chen).

can help the optimization convergence and it can efficiently reduce the gray elements. From an optimization point of view, some different designs could be obtained.

3.2. Sensitivity analysis formulation for fatigue life in the frequency domain

It is essential to derive the sensitivity value of the accumulated damage. We do so by combining the adjoint sensitivity method with the Lagrange multiplier, $\boldsymbol{\lambda}$. First, the differentiation of the accumulated damage is calculated as:

$$\frac{d\left\langle \tilde{D}_{PN}\right\rangle}{d\tilde{\gamma}_e} = \frac{\partial\left\langle \tilde{D}_{PN}\right\rangle}{\partial\tilde{\gamma}_e} + \sum_{n=0}^{4}\frac{\partial\left\langle \tilde{D}_{PN}\right\rangle}{\partial\tilde{D}_e}\frac{\partial\tilde{D}_e}{\partial D_e}\left(\frac{\partial D_e}{\partial E_{p,e}}\frac{\partial E_{p,e}}{\partial m_{n,e}} + \frac{\partial D_e}{\partial p_e}\frac{\partial p_e}{\partial m_{n,e}}\right)\frac{\partial m_{n,e}}{\partial \boldsymbol{\sigma}_{v,e}}\frac{\partial \boldsymbol{\sigma}_{v,e}}{\partial \boldsymbol{\sigma}_e}\frac{\partial \boldsymbol{\sigma}_e}{\partial\tilde{\gamma}_e}$$

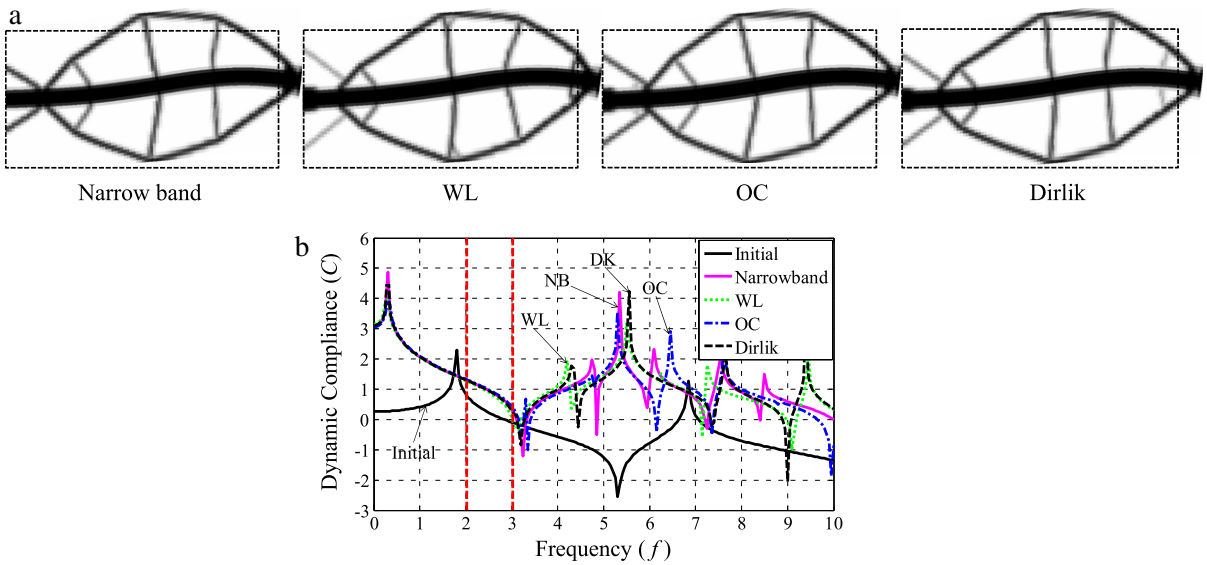

Fig. 35. Deformed shape and FRF (frequency response function): (a) the deformation of the optimal layouts ($SF = 1.0$, WL = Wirsching and Light, OC = Ortiz and Chen) and (b) the FRFs of the results. (Initial curve is Fig. 33(d).)

$$+\sum_{e^*=1}^{NE}\sum_{n=0}^{4}\frac{\partial\left\langle\tilde{D}_{PN}\right\rangle}{\partial\tilde{D}_{e^*}}\frac{\partial\tilde{D}_{e^*}}{\partial D_{e^*}}\left(\frac{\partial D_{e^*}}{\partial E_{p,e^*}}\frac{\partial E_{p,e^*}}{\partial m_{n,e^*}}+\frac{\partial D_{e^*}}{\partial p_{e^*}}\frac{\partial p_{e^*}}{\partial m_{n,e^*}}\right)\frac{\partial m_{n,e^*}}{\partial\boldsymbol{\sigma}_{v,e^*}}\frac{\partial\boldsymbol{\sigma}_{v,e^*}}{\partial\boldsymbol{\sigma}_{e^*}}\frac{\partial\boldsymbol{\sigma}_{e^*}}{\partial\mathbf{U}}\frac{d\mathbf{U}}{d\tilde{\gamma}_e} \tag{26}$$

where the nth momentum of Eq. (5) and the associated PDF function of the eth element of Eq. (6) are denoted by $m_{i,e}$ and p_e, respectively. As the term, $\frac{d\mathbf{U}}{d\tilde{\gamma}_e}$, is difficult to calculate, the following Lagrange multiplier is introduced.

$$\mathbf{K}_D^{\mathrm{T}}\boldsymbol{\lambda}=-\sum_{e^*=1}^{NE}\sum_{n=0}^{4}\frac{\partial\left\langle\tilde{D}_{PN}\right\rangle}{\partial\tilde{D}_{e^*}}\frac{\partial\tilde{D}_{e^*}}{\partial D_{e^*}}\left(\frac{\partial D_{e^*}}{\partial E_{p,e^*}}\frac{\partial E_{p,e^*}}{\partial m_{n,e^*}}+\frac{\partial D_{e^*}}{\partial p_{e^*}}\frac{\partial p_{e^*}}{\partial m_{n,e^*}}\right)\left(\frac{\partial m_{n,e^*}}{\partial\boldsymbol{\sigma}_{v,e^*}}\frac{\partial\boldsymbol{\sigma}_{v,e^*}}{\partial\boldsymbol{\sigma}_{e^*}}\frac{\partial\boldsymbol{\sigma}_{e^*}}{\partial\mathbf{U}}\right)^{\mathrm{T}}. \tag{27}$$

And the final sensitivity analysis can thus be obtained.

$$\frac{d\left\langle\tilde{D}_{PN}\right\rangle}{d\tilde{\gamma}_e}=\frac{\partial\left\langle\tilde{D}_{PN}\right\rangle}{\partial\tilde{\gamma}_e}+\boldsymbol{\lambda}^{\mathrm{T}}\frac{d\mathbf{K}_D}{d\tilde{\gamma}_e}\mathbf{U}+\sum_{n=0}^{4}\frac{\partial\left\langle\tilde{D}_{PN}\right\rangle}{\partial\tilde{D}_e}\frac{\partial\tilde{D}_e}{\partial D_e}\left(\frac{\partial D_e}{\partial E_{p,e}}\frac{\partial E_{p,e}}{\partial m_{n,e}}+\frac{\partial D_e}{\partial p_e}\frac{\partial p_e}{\partial m_{n,e}}\right)\frac{\partial m_{n,e}}{\partial\boldsymbol{\sigma}_{v,e}}\frac{\partial\boldsymbol{\sigma}_{v,e}}{\partial\boldsymbol{\sigma}_e}\frac{\partial\boldsymbol{\sigma}_e}{\partial\tilde{\gamma}_e}. \tag{28}$$

4. Numerical examples

In this section, we solve three TO optimization problems to demonstrate the effect of the accumulated damage calculated by the four damage assessment methods. For the gradient based optimizer, we use the method of moving asymptotes [41].

4.1. Example 1: L-bracket

For the first numerical example, Fig. 11 shows an L-shape bracket structure, which is one of the benchmark problems for stress-based TO. Relevant research has shown that structures with rounded corners are preferred to prevent stress concentration at the corner [14,15,21]. By comparing the optimal layouts of stress-based TO design and our proposed accumulated damage design, we can discuss the validity, unique features, and usefulness of our approach. Fig. 11(a) shows the detailed geometry and boundary conditions. The design domain is discretized by 3600 linear quad elements with the plane stress assumption. The S–N curve based on Eq. (2) in Fig. 11(b) is used, and the mechanical load is constructed by combining the two frequency loads in Fig. 11(c). We chose the mechanical load in Fig. 11(c) to investigate the optimized layouts for a dynamic load whose frequencies are below the first resonance frequency, as shown in Fig. 11(d).

Depending on the value used for the scaling factor, different designs can be obtained. With the present approaches (narrow band solution, Wirsching and Light, Ortiz and Chen, and Dirlik's), some optimal layouts in Fig. 12 can be obtained with 1 as the scaling value in Eq. (25). Fig. 13 shows the deformation shapes of the designs. As shown, some designs similar to those of the stress-based TO method can be obtained, i.e., designs with rounded corners. Note that those four designs

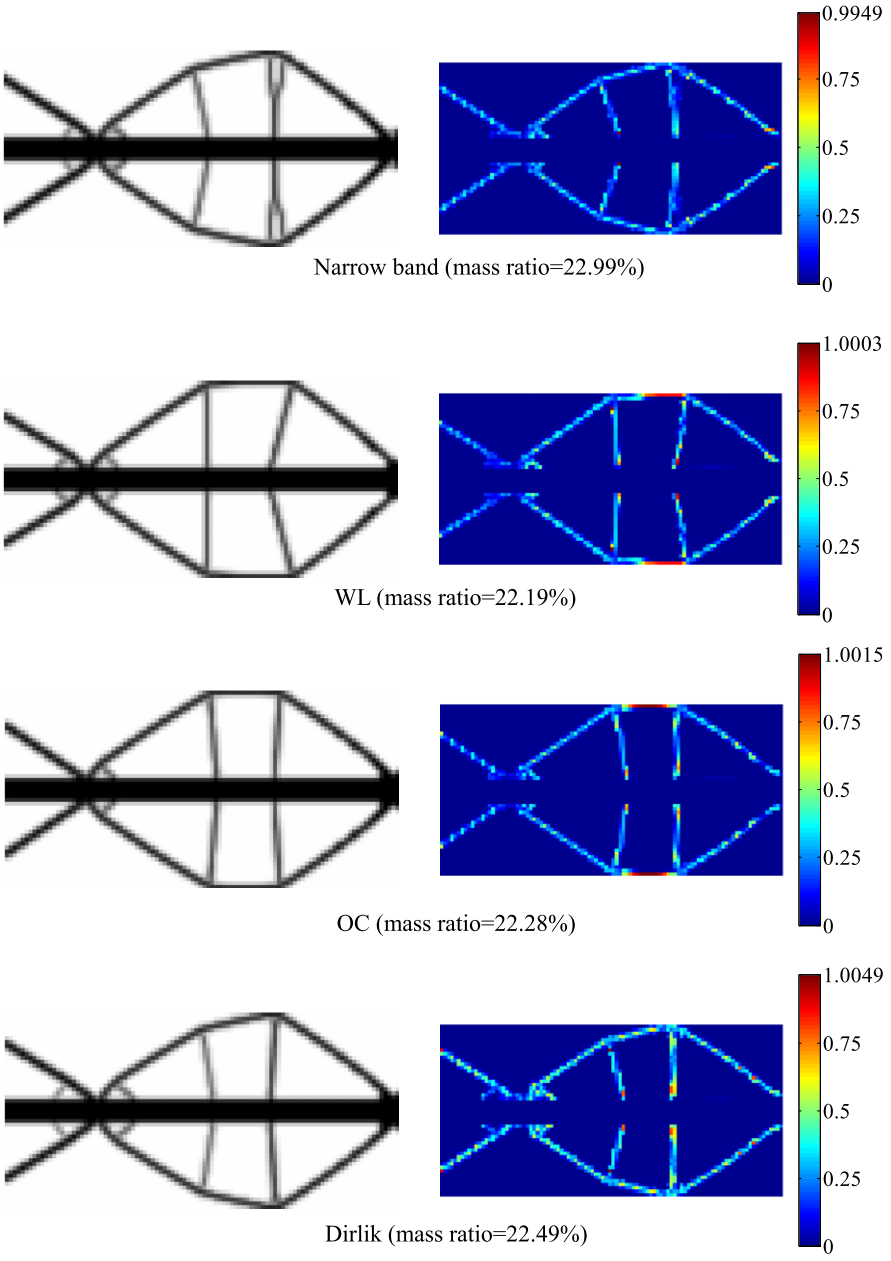

Fig. 36. Optimal layouts considering the fatigue constraint ($SF = 2.0$, WL = Wirsching and Light, OC = Ortiz and Chen).

have smoothed corners to prevent stress concentrations, and the damage of all elements is constrained smoothly. In other words, with 1 for the scaling factor, the optimizer can satisfy the damage constraint related to stress only by removing materials near the corner. Figs. 14 and 16 show the optimized layouts with the four fatigue assessment methods and different scaling factors. Figs. 15 and 17 show the deformations of those designs. It is interesting that the designs with 2 for the scaling factor are similar to those in Fig. 12, but their objective values are also higher, except the result from Dirlik method. It is even more interesting that the designs with 5 for the scaling factor are similar to those of the compliance minimization problems, and it is important to note that those designs also satisfy the damage constraints. As illustrated in Fig. 10, with a higher scaling factor, some higher fatigue constraint values are under-estimated, and consequently an optimizer would decrease the damage values of the other finite elements by reinforcing them. In other words, although the finite elements at the corner sustain higher damage at a few initial optimization iterations, an optimizer with a higher scaling factor reinforces other parts rather than removing materials near the corner. These phenomena or interactions between the scaling factor and the optimizer can be used to obtain optimized layouts converged to solids and voids. In the compliance minimization problem with the SIMP approach, a layout whose design variables are prone to converge to ones or zeros is

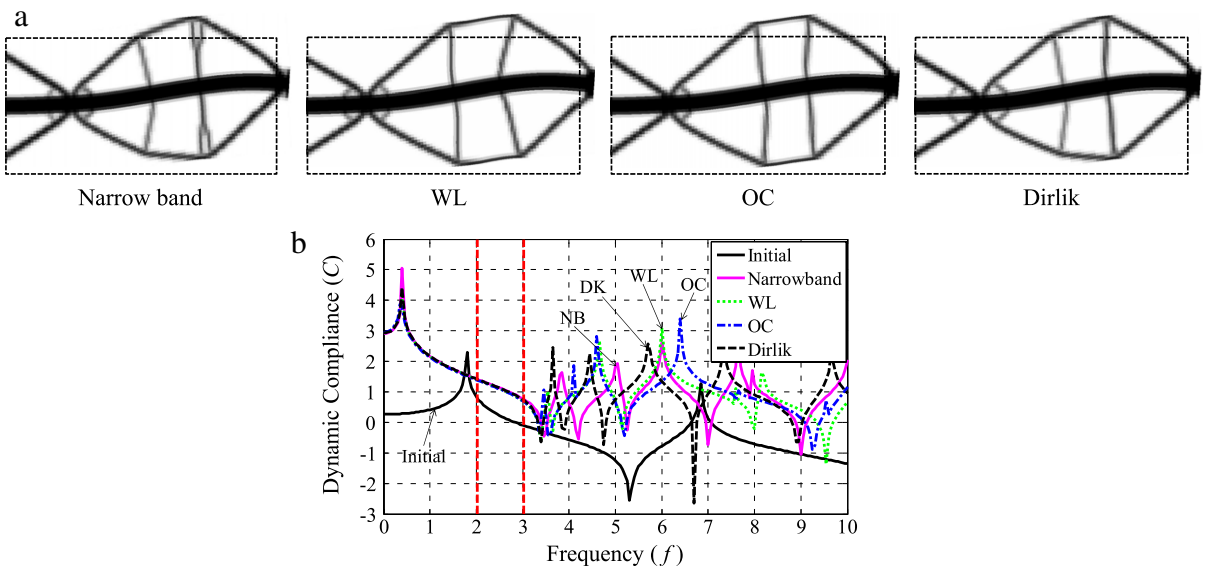

Fig. 37. Deformed shape and FRF (frequency response function): (a) the deformation of the optimal layouts ($SF = 2.0$, WL = Wirsching and Light, OC = Ortiz and Chen) and (b) the FRFs of the results. (Initial curve is Fig. 33(d).)

preferred over un-converged or gray designs. Thus if some gray designs, i.e., designs not fully converged to ones or zeros, are obtained, an alternative approach is optimizing the problem with a higher scaling factor. More important, these examples also demonstrate that to minimize the stress constraint or the fatigue constraint, two design approaches exist. One approach is to remove the materials of finite elements that violate the stress constraint or the fatigue constraint. The other approach is to reinforce the materials of finite elements that violate those constraints. To our knowledge, the first approach has always been emphasized and regarded as a solution because the objective values of the layouts with the first approach are lower than those using the second approach. It is our opinion from an optimization point of view, there may be an alternative third approach not been found yet providing better local optima than the two approaches. And the layouts by the second approach are local optima.

From a fatigue analysis point of view, Dirlik method computes the accumulated damages most accurately among the four methods. To show this difference, we recalculate the damage from the other methods for the optimal layout by the Dirlik method in Fig. 18(d). The maximum damage of the narrow band, WL, and OC methods is 3.1384, 2.3307, and 2.6149, respectively, whereas the maximum value of Dirlik method is 0.9999. This example shows that depending on the assessment method, different designs can be obtained, and Dirlik method is superior to the other methods in terms of accuracy. However, to show the validity of the present approach, the other methods are further tested in the other examples.

Fig. 19 shows the typical optimization histories. As stated, with the scaling factor, the stable optimization can be achievable.

To show the versatility of the present approach, anther mechanical load, whose frequencies are higher than those of the previous example, is applied in Fig. 20. Fig. 21 shows the optimized layouts with the four fatigue constraint methods. All the designs satisfy the damage constraints, but many gray elements exist in Fig. 21. Thus Fig. 22 shows the optimized layouts with 2 for the scaling factor, which shows clearer interpretations of the optimal layouts than the designs in Fig. 21. At the bottom, some resonator structures are observed, along with X-shaped structures at the clamped sides. In particular, sharp corners are obtained because of the effects of the dynamic deformation. In Fig. 23, we can confirm that most largely deformed regions are left part and right lower part. Also the corner part is little deformed than these two parts that are circled in Fig. 23. Therefore the sharp corner appears.

4.2. Example 2: Cantilever beam

Cantilever beam 1

The next numerical example considers the cantilever beam in Fig. 24(a). See the figure for the detailed geometry and boundary conditions. The design domain is 200 mm by 100 mm and is discretized by 5000 linear quad elements. The mechanical load in Fig. 24(c) is applied for 100 s.

As discussed in the first numerical example, we can successfully obtain optimal layouts that satisfy the damage constraint (Figs. 25, 28, and 30). Figs. 27, 29, and 31 show the deformations of the designs. With the higher scaling value, layouts similar to those from the compliance minimization problem can be obtained. To further test the effect of the gray elements, the last design in Fig. 25 is taken. The damage constraint and the volume are computed by varying the 2475th design variable from

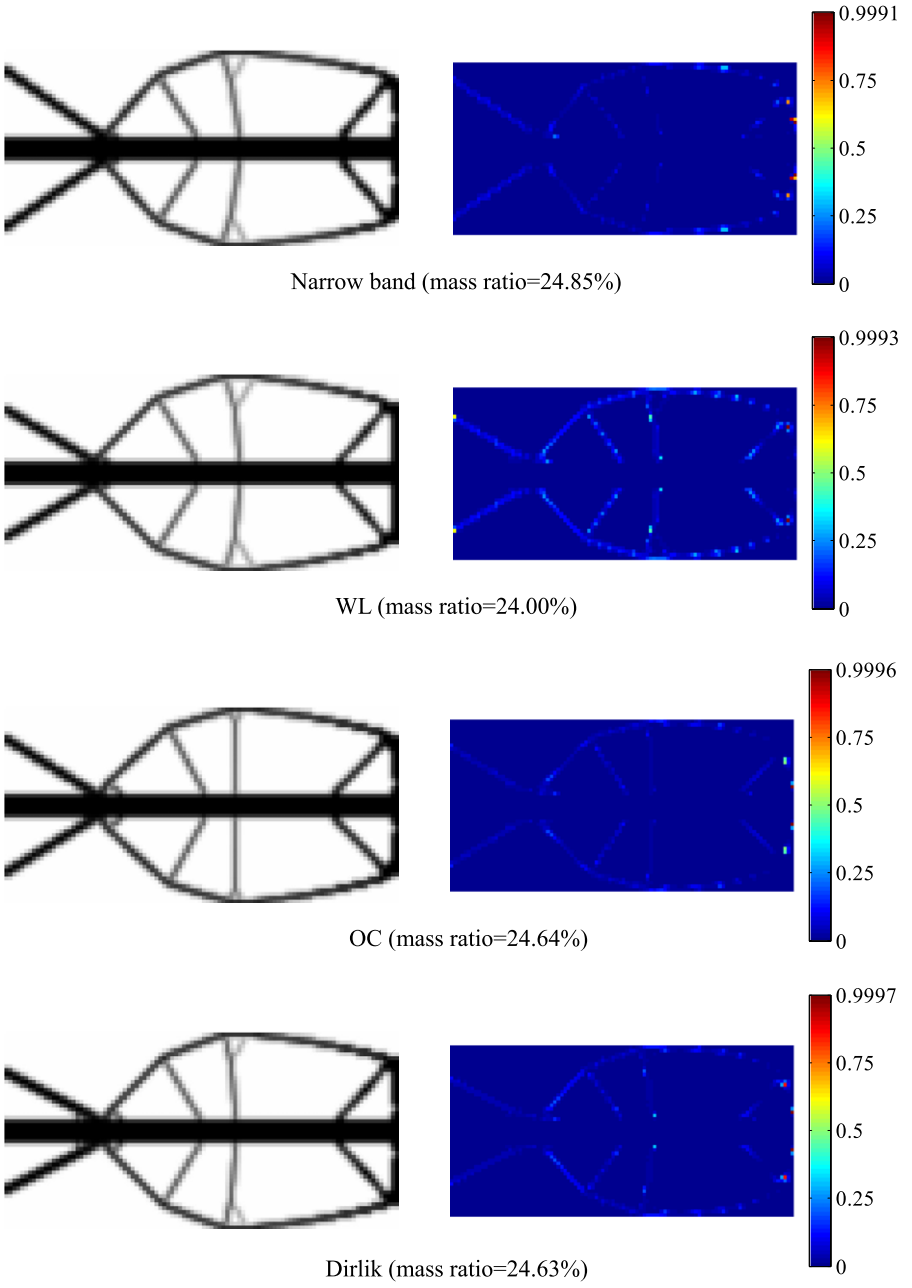

Fig. 38. Optimal layouts considering the fatigue constraint ($SF = 5$, WL = Wirsching and Light, OC = Ortiz and Chen).

0 to 1 in Fig. 26. As illustrated, the damage and the volume are slightly affected. Therefore it requires long optimization iterations.

To compare the optimized designs with the designs from the dynamic compliance minimization problem, Fig. 32 shows the optimal layout for the present damage constraint and the optimal layout minimizing the dynamic compliance subject to the mass constraint (40% here). As illustrated, the optimized layouts from the static or dynamic compliance minimization problem are inferior to the present design in terms of the dynamic fatigue constraint.

Cantilever beam 2

For the next numerical example, we consider the cantilever beam problem with a center reinforcement structure (Fig. 33). One reason for the reinforcement structure is to apply harmonic loads whose frequencies are higher than the first natural frequency. Without the reinforcement, the frequency responses of intermediate designs vary too much for a gradient optimizer to smoothly solve the optimization problem.

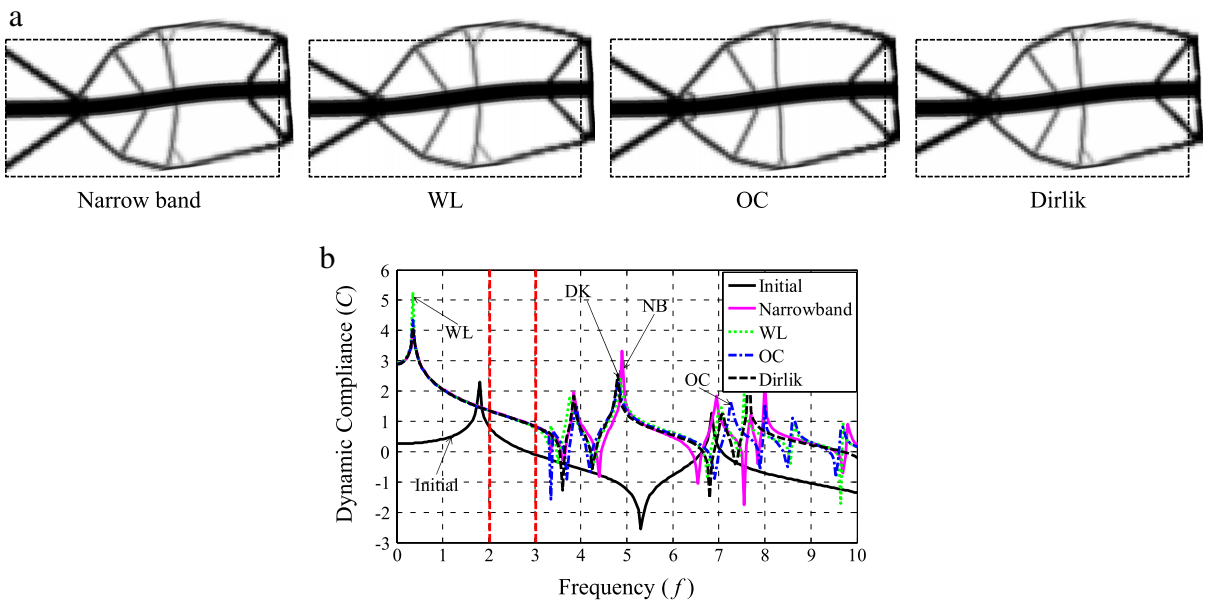

Fig. 39. Deformed shape and FRF (frequency response function): (a) the deformation of the optimal layouts ($SF = 5.0$, WL = Wirsching and Light, OC = Ortiz and Chen) and (b) the FRFs of the results. (Initial curve is Fig. 33(d).)

Figs. 34, 36, and 38 show the optimized layouts with some different scaling factors. All the designs satisfy the damage constraints, and the discussions of the previous examples apply to this problem (see Figs. 35, 37 and 39).

5. Conclusions

This research presents a new TO method that minimizes the volume subject to fatigue life in the frequency domain. The statistical estimation methods for fatigue life (narrow band solution, Wirsching and Light method, Ortiz and Chen method, and Dirlik method) are adopted in the present TO approach; Dirlik method is superior to the others. For successful TO, the p-norm approach and the qp-relaxation method are adopted. In addition, from a structural optimization point of view, the present results show that two approaches to constrain local damage exist. The first approach is to remove materials or densities from design domains whose local damage is too high, and the second approach is to reinforce other domains to minimize extraordinary local damage. By solving some numerical examples, we found that our approach successfully constrains fatigue damage. We also found that when the frequencies of mechanical loads are far smaller than the first natural frequency of the structure, the stress-based topology optimization problem with static loads can be applied.

In conclusion, this research presents a new topology optimization algorithm with structural load that can consider fatigue life in the frequency domain. For future research, the present approach can be extended for some practical engineering fatigue problems caused by repeated thermal shock, fluctuating fluid-induced vibration, or acoustic pressure-induced vibration. Furthermore, the present dynamic fatigue constraints in the frequency domain consider only proportional loads that do not change their principal axes. For future research, it is possible to use some advanced formula to consider the non-proportional load [40].

Acknowledgments

This work was supported by the Human Resources Program in Energy Technology of the Korea Institute of Energy Technology Evaluation and Planning (KETEP), granted financial resource from the Ministry of Trade, Industry & Energy, Republic of Korea (No. 20154030200900), the Research fund of Survivability Technology Defense Research Center of Agency for Defense Development of Korea (No. UD150013ID) and the Global Frontier R&D Program on Center for Wave Energy Control based on Metamaterials funded by the National Research Foundation under the Ministry of Science, ICT & Future Planning, Korea (No. 2014063711).

References

[1] J.A. Bannantine, J.J. Comer, J.L. Handrock, Fundamentals of Metal Fatigue Analysis, Prentice Hall, Englewood Cliffs, NJ, 1990.
[2] S. Suresh, Fatigue of Materials, second ed., Cambridge University Press, Cambridge, New York, 1998.
[3] N. Bishop, The Use of Frequency Domain Parameters to Predict Structural Fatigue, University of Warwick, 1988.
[4] N.W. Bishop, F. Sherratt, Finite Element Based Fatigue Calculations, NAFEMS, 2000.

[5] P.H. Wirsching, M.C. Light, Fatigue under wide band random stresses, J. Struct. Div. 106 (1980) 1593–1607.
[6] K. Ortiz, N. Chen, Fatigue damage prediction for stationary wideband random stresses, in: Proceedings of the 5th International Conference on Applications of Statistics and Probability in Soil and Structural Engineering, ICASP 5, 1987, pp. 309–316.
[7] T. Dirlik, Application of computers in fatigue analysis. University of Warwick, 1985.
[8] A. Halfpenny, A frequency domain approach for fatigue life estimation from finite element analysis, Key Eng. Mater. 167 (1999) 401–410.
[9] Y.-L. Lee, M.E. Barkey, H.-T. Kang, Metal Fatigue Analysis Handbook: Practical Problem-Solving Techniques for Computer-Aided Engineering, Butterworth-Heinemann, Waltham, MA, 2012.
[10] G.I.N. Rozvany, Difficulties in truss topology optimization with stress, local buckling and system stability constraints, Struct. Optim. 11 (1996) 213–217.
[11] R.J. Yang, C.J. Chen, Stress-based topology optimization, Struct. Optim. 12 (1996) 98–105.
[12] P. Duysinx, M.P. Bendsoe, Topology optimization of continuum structures with local stress constraints, Internat. J. Numer. Methods Engrg. 43 (1998) 1453–1478.
[13] G. Allaire, F. Jouve, H. Maillot, Topology optimization for minimum stress design with the homogenization method, Struct. Multidiscip. Optim. 28 (2004) 87–98.
[14] J. Paris, F. Navarrina, I. Colominas, M. Casteleiro, Topology optimization of continuum structures with local and global stress constraints, Struct. Multidiscip. Optim. 39 (2009) 419–437.
[15] J. París, F. Navarrina, I. Colominas, M. Casteleiro, Block aggregation of stress constraints in topology optimization of structures, Adv. Eng. Softw. 41 (2010) 433–441.
[16] M. Burger, R. Stainko, Phase-field relaxation of topology optimization with local stress constraints, SIAM J. Control Optim. 45 (2006) 1447–1466.
[17] M. Bruggi, P. Venini, A mixed FEM approach to stress-constrained topology optimization, Internat. J. Numer. Methods Engrg. 73 (2008) 1693–1714.
[18] M. Bruggi, On an alternative approach to stress constraints relaxation in topology optimization, Struct. Multidiscip. Optim. 36 (2008) 125–141.
[19] M. Bruggi, P. Duysinx, Topology optimization for minimum weight with compliance and stress constraints, Struct. Multidiscip. Optim. 46 (2012) 369–384.
[20] K. Svanberg, M. Werme, Sequential integer programming methods for stress constrained topology optimization, Struct. Multidiscip. Optim. 34 (2007) 277–299.
[21] C. Le, J. Norato, T. Bruns, C. Ha, D. Tortorelli, Stress-based topology optimization for continua, Struct. Multidiscip. Optim. 41 (2010) 605–620.
[22] G.Y. Qiu, X.S. Li, A note on the derivation of global stress constraints, Struct. Multidiscip. Optim. 40 (2010) 625–628.
[23] M. Kocvara, M. Stingl, Solving stress constrained problems in topology and material optimization, Struct. Multidiscip. Optim. 46 (2012) 1–15.
[24] Y.J. Luo, Z. Kang, Topology optimization of continuum structures with Drucker–Prager yield stress constraints, Comput. & Structures 90–91 (2012) 65–75.
[25] E. Lee, K.A. James, J.R.A. Martins, Stress-constrained topology optimization with design-dependent loading, Struct. Multidiscip. Optim. 46 (2012) 647–661.
[26] S.H. Jeong, S.H. Park, D.H. Choi, G.H. Yoon, Topology optimization considering static failure theories for ductile and brittle materials, Comput. & Structures 110 (2012) 116–132.
[27] S.H. Jeong, D.-H. Choi, G.H. Yoon, Fatigue and static failure considerations using a topology optimization method, Appl. Math. Model. 39 (2015) 1137–1162.
[28] A. Takezawa, G.H. Yoon, S.H. Jeong, M. Kobashi, M. Kitamura, Structural topology optimization with strength and heat conduction constraints, Comput. Methods Appl. Math. 276 (2014) 341–361.
[29] B. Desmorat, R. Desmorat, Topology optimization in damage governed low cycle fatigue, C. R. Mec. 336 (2008) 448–453.
[30] E. Holmberg, B. Torstenfelt, A. Klarbring, Global and clustered approaches for stress constrained topology optimization and deactivation of design variables, 2013.
[31] C.L.J. Norato, A method for fatigue-based topology optimization, in: Proc. 10th World Congress on Structural and Multidisciplinary Optimization, Orlando, Florida, USA, 2013.
[32] K. Suzuki, N. Kikuchi, A homogenization method for shape and topology optimization, Comput. Methods Appl. Math. 93 (1991) 291–318.
[33] M.P. Bendsøe, O. Sigmund, Topology Optimization: Theory, Methods, and Applications, Springer, Berlin, New York, 2003.
[34] O. Sigmund, A 99 line topology optimization code written in Matlab, Struct. Multidiscip. Optim. 21 (2001) 120–127.
[35] G.H. Yoon, J.S. Jensen, O. Sigmund, Topology optimization of acoustic-structure interaction problems using a mixed finite element formulation, Internat. J. Numer. Methods Engrg. 70 (2007) 1049–1075.
[36] G.H. Yoon, Maximizing the fundamental eigenfrequency of geometrically nonlinear structures by topology optimization based on element connectivity parameterization, Comput. & Structures 88 (2010) 120–133.
[37] G.H. Yoon, J.C. Heo, Constraint force design method for topology optimization of planar rigid-body mechanisms, Comput. Aided Des. 44 (2012) 1277–1296.
[38] J.C. Heo, G.H. Yoon, Size and configuration syntheses of rigid-link mechanisms with multiple rotary actuators using the constraint force design method, Mech. Mach. Theory 64 (2013) 18–38.
[39] G. Cheng, Z. Jiang, Study on topology optimization with stress constraints, Eng. Optim. 20 (1992) 129–148.
[40] S.-B. Lee, Out-of-phase, combined bending and torsion fatigue of steels, in: M.W. Brown, K.J. Miller (Eds.), Proc. Biaxial and Multiaxial Fatigue, EGF 3, Mechanical Engineering Publications, 1989, pp. 621–634.
[41] K. Svanberg, The method of moving asymptotes—a new method for structural optimization, Internat. J. Numer. Methods Engrg. 24 (1987) 359–373.